TEKNILLINEN KORKEAKOULU
Sähkö- ja tietoliikennetekniikan osasto

Kimmo Kalliola

TESTBED FOR ADAPTIVE ARRAY ANTENNAS

Diplomityö, joka on jätetty opinnäytteenä tarkastettavaksi
diplomi-insinöörin tutkintoa varten Espoossa 21.2.97

Työn valvoja P. Vainikainen
Apulaisprofessori Pertti Vainikainen

HELSINKI UNIVERSITY OF TECHNOLOGY **ABSTRACT OF THE MASTER'S THESIS**

Author:	Kimmo Kalliola	
Name of the thesis:	Testbed for adaptive array antennas	
Date:	February 21, 1997	**Number of pages:** 87
Department:	Department of Electrical and Communications Engineering	
Professorship:	Radio Engineering	
Supervisor:	Associate Professor Pertti Vainikainen	
Instructor:	M.Sc. Veli Voipio	

In this master's thesis adaptive array antennas like those used at base stations of cellular networks are studied. Adaptive base station antennas provide advantages compared to the existing sectored or omnidirectional antenna solutions in terms of enhanced capacity, decreased transmission power levels, and increased coverage.

At first the benefits of adaptivity as well as possible approaches to the implementation are discussed. Introduction to array antennas and radiation properties of different array geometries are presented next. Also techniques of pattern optimization v. number of array elements and size and geometry of the array are investigated.

A testbed has been built to investigate different array configurations. It is based on a complex wideband radio channel sounder and a fast RF switch. The testbed provides both the incidence angle and delay information of the received signal component and thus allows two-dimensional characterization of the radio channel in realistic environments. The built device can be used in the analysis of antenna arrays and radio channels in various radio systems. As an example, the testbed allows measuring of complex impulse responses for a 16-element array with 17 ns delay resolution, and a delay range of 4.3 μs for 26 m/s mobile speed. The performance of the system has been studied by test measurements.

The testbed has also been evaluated with practical channel measurements with an 8-element prototype array. The results indicate that the system works well and the components of the received signal with different directions of arrival and time delays can be separated with 13° angular resolution. The developed system provides a novel approach to the two-dimensional analysis of the radio channel.

Keywords: Adaptive antenna, array antenna, channel sounding, mobile communications

TEKNILLINEN KORKEAKOULU **DIPLOMITYÖN TIIVISTELMÄ**

Tekijä:	Kimmo Kalliola
Työn nimi:	Adaptiivisten ryhmäantennien testausjärjestelmä
Päivämäärä:	21.2.1997 **Sivumäärä:** 87
Osasto:	Sähkö- ja tietoliikennetekniikan osasto
Professuuri:	Radiotekniikka
Työn valvoja:	Apulaisprofessori Pertti Vainikainen
Työn ohjaaja:	DI Veli Voipio

Tässä diplomityössä tutkitaan esim. solukkoradioverkkojen tukiasemille soveltuvia adaptiivisia ryhmäantenneja. Adaptiivisilla tukiasema-antenneilla saavutetaan monia etuja nykyisten järjestelmien antenniratkaisuihin verrattuna. Saavutettavia parannuksia ovat mm. suurempi kapasiteetti, matalammat lähetystehot ja laajempi peittoalue.

Aluksi tarkastellaan adaptiivisten antennien mahdollisia toteutustapoja ja niiden tarjoamia etuja. Seuraavaksi käsitellään ryhmäantennien teoriaa ja ryhmän geometrian vaikutusta antennin säteilyominaisuuksiin. Myös säteilykuvion optimointia elementtien lukumäärän sekä ryhmän koon ja geometrian suhteen tarkastellaan.

Erilaisten antenniryhmien tutkimiseksi on rakennettu testausjärjestelmä. Järjestelmä koostuu kompleksisesta laajakaistaisesta radiokanavaluotaimesta ja RF-kytkimestä. Laitteen avulla voidaan vastaanotetusta signaalikomponentista laskea sekä tulokulma että viive. Tämä tarjoaa mahdollisuuden radiokanavan kaksiulotteiseen mallintamiseen todellisissa ympäristöissä. Rakennettua laitteistoa voidaan käyttää antenniryhmien ja radiokanavien analysointiin erilaisissa radiojärjestelmissä. Laitteiston avulla voidaan mitata kompleksiset impulssivasteet esimerkiksi 16-elementtisestä antenniryhmästä 17 ns viiveresoluutiolla ja 4,3 μs maksimiviiveellä mobiiliaseman nopeudella 26 m/s. Laitteiston suorituskykyä on tutkittu testimittausten avulla.

Laitteiston toimintaa käytännössä on testattu todellisilla kanavamittauksilla 8-elementtisen antenniryhmän prototyypin avulla. Tulokset osoittavat, että järjestelmä toimii hyvin, ja eri suunnista eri aikaviiveillä vastaanotetut signaalit voidaan erottaa toisistaan 13° kulmaresoluutiolla. Kehitetty menetelmä tarjoaa uusia mahdollisuuksia radiokanavan kaksiulotteiseen mallintamiseen.

Avainsanat: Adaptiivinen antenni, ryhmäantenni, kanavaluotaus, siirtyvä tietoliikenne

Preface

This master's thesis work has been carried out in Radio Laboratory at Institute of Radio Communications (IRC), Helsinki University of Technology (HUT). The work is part of an IRC project called New Radio Systems and Their RF Engineering (SARF) funded by the Academy of Finland and HUT. I express my gratitude for having had the possibility to participate in the project.

I would like to thank my supervisor, Associate Professor Pertti Vainikainen for his numerous ideas and suggestions concerning the work. I also thank Veli Voipio for his comments. In addition, all the Radio Laboratory people deserve thanks for their help and support during this work.

I thank Jani Ollikainen for the many interesting and entertaining discussions. My parents I wish to thank for their support during my entire studies. Finally, I would like to thank my girlfriend Satu for her support during this work and patience in the last months.

Helsinki, February 21, 1997

Kimmo Kalliola

Table of contents

List of symbols

a	signal amplitude
A	amplitude of electrical field
b	signal amplitude
BER	bit error rate
BW	bandwidth
c	speed of light
C	coupling coefficient
CNR	carrier-to-noise ratio
d	element spacing
D	directive gain, directivity
e	element radiation pattern
e_i	isolated element radiation pattern
f	array factor, frequency
f_0	center frequency
f_c	chip frequency
f_D	Doppler frequency
f_m	measurement rate
$f_{m,a}$	array measurement rate
$f_{m,e}$	element measurement rate
f_s	sample rate
F	radiation pattern
$\mathcal{F}$	Fourier transform
g	radiation pattern of element in array
H_{feed}	transmission function
$HPBW$	half-power beamwidth
I	interference power
k	wave number
K	scaling factor
L	path loss, array length
L_c	code length
m,n	element index
M,N	number of array elements
N_R	number of reflections
P_n	noise power
P_{rad}	radiation power
Q_r	radiation quality factor
R	circle radius
$\boldsymbol{r}$	position vector
r_m	measured impulse response
s	element signal
S	signal power, coupling coefficient
SLL	sidelobe level
$SINR$	signal-to-interference and noise ratio
SIR	signal-to-interference ratio
SNR	signal-to-noise ratio

t_m	continuous measurement time
$\boldsymbol{u_r}$	unit vector
v	speed of mobile
w	signal weight
W	radiation intensity per unit solid angle
W_{coh}	coherence bandwidth
XPD	cross polarization discrimination
α	angle of incidence, phase shift
β	phase shift
δ	phase shift
Δ	beam mispointing angle
Δf	bandwidth
$\Delta\phi$	cumulative phase error
$\Delta\phi_{\text{rms}}$	rms phase error
ε_T	taper efficiency
θ	elevation angle
θ_0	elevation angle of main beam
θ_p	grating lobe angle
$\Theta_{3\text{dB}}$	3 dB beamwidth in *yz*-plane
Θ_{x0}	3 dB beamwidth of linear array along *x*-axis
Θ_{y0}	3 dB beamwidth of linear array along *y*-axis
κ	proportionality coefficient
λ	wavelength
σ	rms error
σ_a	rms amplitude error
σ_n^2	noise variance
σ_p	rms phase error
τ	time delay
τ_{max}	delay range
τ_{min}	delay resolution
ϕ	azimuth angle
ϕ_0	azimuth angle of main beam
$\Psi_{3\text{dB}}$	3 dB beamwidth in *xy*-plane
Ω_A	beam solid angle

List of abbreviations

ADC	analog-to-digital converter
AGC	automatic gain control
BS	base station
CDMA	code-division multiple access
DBF	digital beamforming
DECT	Digital European Cordless Telephone
DOA	direction of arrival
DS	direct sampling
DSB	double sideband
DSP	digital signal processing
FDD	frequency-division duplex
GSM	Global System for Mobile communications, Groupe Special Mobile
HUT	Helsinki University of Technology
I	in-phase component
IF	intermediate frequency
IR	impulse response
IRC	Institute of Radio Communications
MRA	minimum redundancy array
MS	mobile station
LMS	least mean squares
LOS	line-of-sight
OFDMA	orthogonal frequency-division multiple access
PN	pseudo noise
PPS	pulse-per-sequence
Q	quadrature component
RF	radio frequency
RLS	recursive least squares
SAW	surface acoustic wave
SB	switched-beam
SDMA	space-division multiple access
SSB	single sideband
UMTS	Universal Mobile Telecommunications System
TDMA	time-division multiple access
TTL	transistor-transistor logic

1 Introduction

The need for mobile telecommunication is increasing rapidly and the existing systems are meeting their capacity limits. Reducing cell sizes and building additional cell sites and base stations is time consuming and expensive. Besides, as cells become small, the number of handovers required for serving a moving mobile becomes impractically large causing degradation of service quality.

This has lead to a search for new system solutions capable of serving the growing number of users. One interesting candidate is the spatial separation of users by the employment of adaptive antennas at the base stations of networks. Adaptive or smart antenna is an array antenna capable of modifying its radiation pattern, frequency response, or other parameters while the antenna is operating.

In cellular networks adaptive base station antennas provide advantages compared to the existing sectored or omnidirectional antenna solutions in terms of enhanced capacity, decreased transmission power levels, and increased coverage. The users in different angular positions from the base station can be served in the same traffic channel, which significantly increases the spectral efficiency of the system. In complex multipath environments the time dispersion and co-channel interference can be decreased by receiving only the strongest signal path from a specific mobile user. The narrow antenna beams provide additional gain making it possible to lower the transmission levels in mobile-to-base direction and thus increase the critical battery lifetime of handportable devices. Alternatively the range of one base station can be increased without increasing the transmission power levels.

The purpose of this work is to determine the issues related to adaptive antennas and to develop and evaluate a test system for studying the requirements of the antenna implementation. The effects of antenna parameters such as the number of array elements, the spacing between the elements, and the array geometry on the performance of adaptive antennas are of interest.

A testbed will be developed for the analysis of different array configurations as well as signal propagation in mobile environments. The testbed will be based on a 2.154 GHz complex wideband radio channel sounder and a fast RF switch. The system will be evaluated with test measurements and practical experiments in real environments.

The thesis is organized as follows. Chapter 2 presents the topics related to antenna adaptivity from the radio system point of view. Theory of array antennas is given in Chapter 3 as well as possible implementation strategies of adaptive arrays. Chapter 4 describes the built antenna testbed. The performance of the testbed is investigated in terms of maximum mobile speed and accuracy of the direction of the received signals. First practical measurements using a prototype array are presented in Chapter 5. Finally, the conclusions are drawn in Chapter 6.

2 Adaptive antennas in mobile communication systems

2.1 Adaptive antenna

The operation of adaptive antennas relies basically on steering the main beam towards the wanted signal and the pattern nulls towards the interferers. The idea of antenna adaptivity is not new. Adaptive self-phased arrays have been applied to radars for over thirty years [1]. Until today, the lack of fast adaptive signal processing techniques has prevented the more general use of adaptive antennas. The recent progress in the fields of integrated circuit technology and digital computing is making it possible to implement very complex systems with moderate cost.

2.2 Advantages of adaptivity

When compared to the existing systems, the adaptive base station (BS) antennas in cellular networks provide advantages in several areas. The most important of the presumed benefits are

- enhanced system capacity
- increased radio coverage
- decreased transmission power

Of these three, the first one is often considered the most important because of the growing number of users. The second offers the possibility to reduce costs by enlarging the cell sizes in low traffic density areas. The last is favored by the mobile equipment designers trying to maximize the battery lifetimes of the devices. The following sections cover each of these subjects in more detail.

2.2.1 Capacity

The main purpose of using adaptive array antennas at base stations of cellular networks is to increase the system capacity by increasing the spectral efficiency. The frequency band allocated for mobile communication is limited. This means that the number of radio channels and users per area is also limited. To use the available radio spectrum efficiently, several modulation and access methods have been developed. In digital systems these consist of e.g. time-division multiple access (TDMA), code-division multiple access (CDMA), and orthogonal frequency-division multiple access (OFDMA) [2,3]. Still, there is a growing need for more capacity in high traffic areas where the networks are interference limited. New modulation and access methods are constantly being sought.

In mobile cellular systems the traffic channels allocated for one cell are used again in another cell. The reuse distance is chosen so that the co-channel interference is small enough not to disturb the signal. System capacity can be increased by reducing the cell sizes and lowering the transmission power levels. This is however costly, because new base stations have to be built. The increase of capacity obtained by the use of adaptive antennas comes from reducing the interference (co- and adjacent channel) from other users. The techniques to implement this in both directions are described in the next two sections.

Uplink

In the mobile (MS) - BS direction (uplink) the interference from other users can be rejected by using an array of antenna elements accompanied by powerful signal processing. The desired signal can be received and the interfering signals rejected by optimally combining different signal paths having different propagation statistics due to differ-

ences in direction of arrival, polarization and antenna position (see Sec. 2.4). This can be thought as pointing antenna beams in the desired directions and pattern nulls in the directions of interferers. Figure 2.1 shows a schematic figure of a cellular network with base stations in the center of each cell. The signals transmitted by mobiles in one cell are received also in the BS of the adjacent cell, supposing the frequencies are the same, or close to each other (Fig. 2.1(a)). If the base station can produce narrow beams and deep nulls in the radiation pattern, the interference level can be substantially reduced (Fig. 2.1(b)).

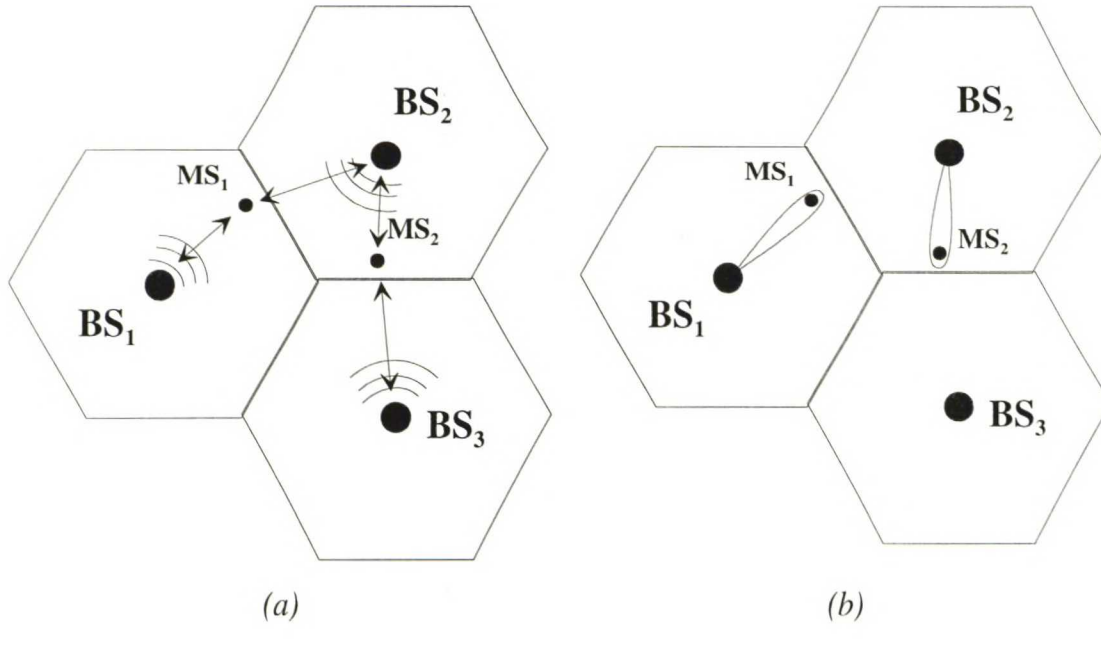

Figure 2.1. *Co- and adjacent channel interference in cellular system. (a) omnidirectional BS antennas. (b) adaptive BS antennas.*

In a micro-cellular environment, where scatterers exist close to the base station, the reflections cause the multipath components of the transmitted signal to be received from different angles (α_i), as presented in Fig. 2.2. Because of the differences in the lengths of the propagation paths and dissimilar reflections, diffractions, and path loss (L), the components also have different time delays (τ) and amplitudes.

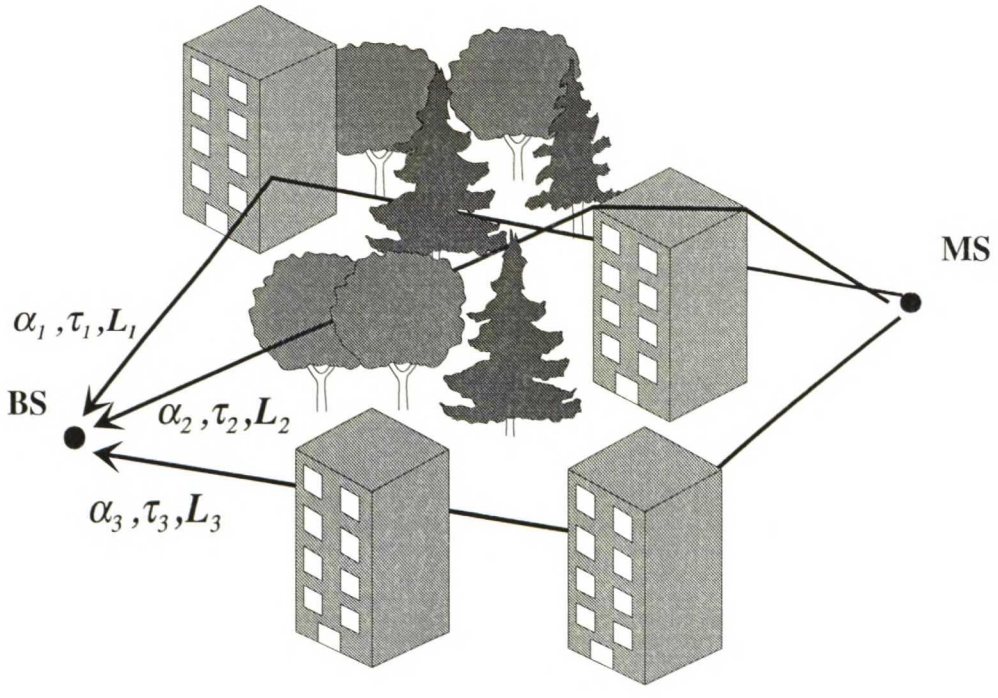

Figure 2.2. *Multipath propagation.*

If an adaptive BS antenna can be used to receive only the strongest multipath and to reject the others, the signal delay spread is reduced. This reduces the intersymbol interference particularly detrimental in the case of high data-rate transmission. Smaller time dispersion offers the possibility to use mobile systems with high bit-rates in difficult environments where it otherwise might not be possible [4]. The critical factor is the channel delay spread v. symbol length. In addition to the multipath rejection, also combining of multipath components is possible.

Downlink

In the BS - MS direction (downlink) the user separation can be accomplished by directing the antenna beam towards one specific user or a group of users at a time. Focusing the radio energy to narrow beams and creating radiation nulls towards undesired mobiles reduce the total interference level of the system. The use of directional beam forming techniques in the downlink enables either smaller channel reuse distances between cells (Fig. 2.1), or alternatively reuse within one cell often referred to as space-division multiple access (SDMA). The two approaches with Global System for Mobile communications (GSM) system are simulated in [5]. It is stated that the former applying

inter-cell nulling performs better provided that efficient uplink power control is available. This is due to the potentiality of the BS to identify the mobiles in adjacent cells suffering from its interference. In the existing frequency-division duplex (FDD) systems the downlink beamforming is somewhat more difficult than the uplink adaptation. This is because the radio channel properties are frequency dependent. The difference between two received signal frequencies having some correlation level is defined as the coherence bandwidth (W_{coh}). It is inversely proportional to the signal delay spread in the channel. In typical mobile channels W_{coh} is considerably smaller than the duplex separation.

An important advantage of adaptive antennas is that the spatial separation of the users can be added to the existing multiple access methods. The implementation and benefits may however become different in different systems and also different radio environments (see Sec. 2.6).

2.2.2 Coverage

In low traffic density areas adaptive base station antennas with narrow directive beams can increase the network coverage. In other words, an equivalent user capacity compared to existing schemes can be achieved with fewer cell sites. This reduces the network infrastructure costs.

2.2.3 Power

Due to the higher antenna gains provided by narrow beams the mobile transmission power levels can be decreased to achieve equal coverage. This results in longer battery lifetimes. Of course the choice between the power and the range is always a compromise.

Several studies exist e.g. [4,6,7] where simulations and experiments have shown good agreement in the aspects discussed above.

2.3 DIFFERENT ADAPTATION STRATEGIES

Adaptive antennas can be divided into three categories depending on the amount of signal processing power employed. The actual radiating part can be the same in each of the three. The difference is in the antenna control system. From the simplest one to the most complex the antenna types are

- switched-beam antenna
- beamforming antenna
- adaptive array

The first two types can be used in both uplink and downlink provided that the radio channel is reciprocal and that directional information of the mobile distribution is available. They also require the response of the antenna (directional, frequency) to be known. The last can be considered as an array of sensor elements more than an array antenna in its conventional meaning. The different types of adaptive antennas are presented in the following sections.

2.3.1 Switched-beam antenna

The switched-beam antenna (SB-antenna) has a radiation pattern consisting of a set of beams with fixed pointing directions. It uses a switching network and a beamforming matrix to form beams in radiation pattern each corresponding to one output port of the matrix. One or more beams can be chosen at a time by switching between the output ports. Figure 2.3 presents the operation of the switched-beam antenna.

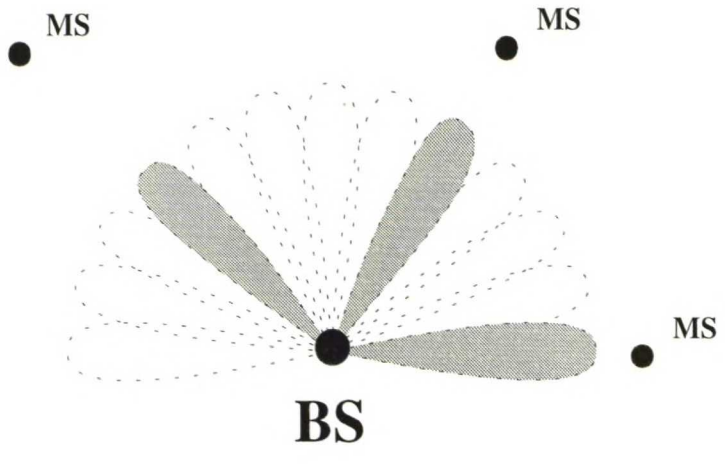

Figure 2.3. *Switched-beam antenna.*

The SB-antenna is less complex than the adaptive array but still useful for the spatial separation of users. Experimental tests in heavy and light urban environments [8] have shown that average system gain improvements of 3 and 5 dB compared to a conventional three sector BS antenna can be achieved by a directional array with 12 and 24 fixed beams, respectively. Another significant benefit over the adaptive array is the capability of operating in both up- and downlink directions. This however requires reciprocal radio channel, which in FDD systems typically means line-of-sight (LOS) channel. This is due to the multipath radio channel with scattering and reflections being frequency dependent. The operation of the SB-antenna is based on the knowledge of angular locations of the users relative to the base station. The information can be obtained e.g. from a higher system level [9].

2.3.2 Beamforming antenna

The beamforming antenna presented in Fig. 2.4 can be thought as an extension of the SB-antenna. It is capable of producing multiple beams and/or nulls.

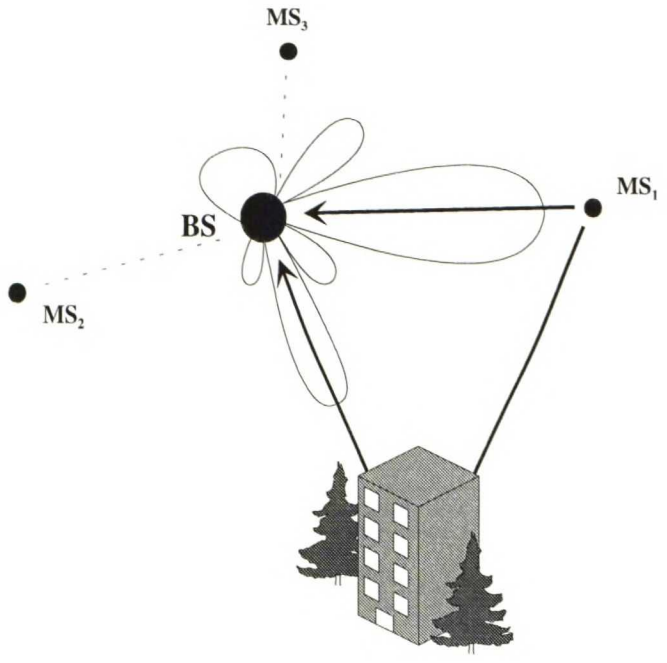

Figure 2.4. *Beamforming antenna.*

The beamforming can be realized by adjusting the amplitudes and phases of the element signals in the RF by controlling the beamforming matrix, or using digital signal processing (DSP) in the baseband. The RF approach leads to less hardware and thus substantial savings in manufacturing costs since only one up- / downconverting unit is needed. If, in turn, the beamforming is made by DSP, direction of arrival (DOA) estimation techniques can be exploited. The beamforming antenna has the benefits of the SB-antenna plus an additional degree of freedom in radiation pattern creation. The following two sections describe the basic beamforming techniques related to the cellular system.

Beam steering

At first, the most obvious adaptation strategy seems to be directing narrow beams towards desired users. In reception, the most important efficiency measure, signal-to-interference and noise ratio (*SINR*), would however be maximized only if no interferers existed and the only noise present were due to the receiver's circuit noise. The received signal power would be maximized, the noise power remaining constant [10]. This is due

to the most harmful interference being caused by the other mobiles and thus received from narrow angles in a typical cellular environment.

Null steering

The *SINR* is calculated through dividing the received signal power by the received interference and noise power:

$$SINR = \frac{S}{I + P_n} = \frac{S}{\sum_{i=1}^{i_0} I_i + P_n} \tag{2.1}$$

where S is the desired signal power, I_i is the interference power caused by the i^{th} interfering mobile, i_0 is the number of interferers, and P_n is the spatially white noise power. When several interfering sources exist, the best improvement in *SINR* is achieved by decreasing the denominator in (2.1). This can be done by placing nulls in the directions of the interferers. An array of N elements can produce (N-1) nulls and thus in theory cancel (N-1) interfering signals. The null steering however causes other also pattern deformations, which have to be considered.

2.3.3 Adaptive array

The adaptive array can be defined as an antenna that modifies its radiation pattern, frequency response, or other parameters, by means of internal feedback control while the antenna is operating [11]. It is the most complex one of the three presented antenna types and limited to reception only. The adaptive array can be thought as an optimal combining antenna, i.e. a group of sensor elements each receiving the same signal with different phase, amplitude, polarization, and noise characteristics depending on the direction of arrival and path loss due to the radio channel. An optimal combination of the sensor signals is computed containing all the information of the desired signal present in the antenna input. The optimal combining of element signals can be thought as forming unique radiation patterns (amplitude, phase and polarization patterns) to serve each mobile user. It ideally corresponds to maximizing the gain in the desired directions and placing nulls in the directions of interference. This type of antenna is defined as 'the

smart antenna' [12]. When digital signal processing is added behind the antenna, the traditional concept of antenna radiation pattern is loosing its meaning. The measure of the signal quality used for the optimal signal combining is the *SINR*. The gain in signal-to-interference ratio (*SIR*) achieved by an adaptive array using the recursive least squares (RLS) algorithm has been simulated in [12]. It is shown through ray tracing simulations that the gain due to the adaptive array is from 10 to 15 dB for original *SIR* values of 29 dB to 2 dB, respectively.

An adaptive array consists of an array of antenna elements and a real-time signal processing unit for setting the phase and amplitude characteristics of different element signals i.e. multiplying the signals by complex coefficients. One receiver is needed for each antenna element because the adaptive signal processor weighting the signals operates in baseband. Figure 2.5 presents the operation of the adaptive array.

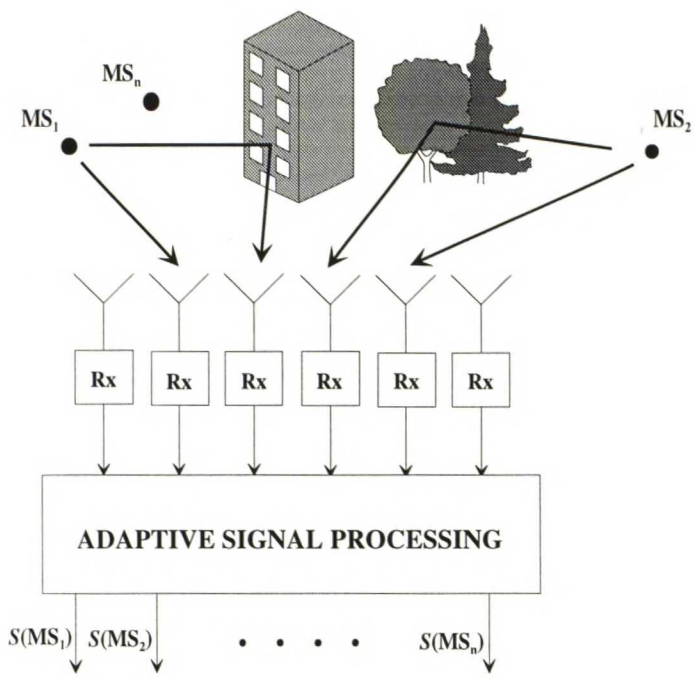

Figure 2.5. *Adaptive array.*

Adaptive algorithms

The phase and amplitude shifts in signals for different elements are determined by a signal processor. Three types of methods exist for this task: steering vector based methods,

reference signal based methods and blind algorithms [13]. The main difference between these algorithms is that the first exploits array response information and thus requires precise knowledge of the array properties. The last two are insensitive to the imperfections in the array geometry or to the mutual coupling effects between elements.

The steering vector based methods require either the employment of a DOA estimation procedure or other a priori information about the mobile transmitter locations (useful if LOS exists). One example of a method of this kind is the Howells-Applebaum beamformer [14]. The reference signal based methods consist of the least mean-square (LMS) algorithm and its variants: (RLS,QRLS,NMLS,SQRLS) [15]. They are based on the minimization of the mean-square of the difference between the received signal and the reference signal. Thus, a reference signal having a high correlation with the desired signal has to be generated. In digital systems a training sequence can be applied in each transmitting mobile. The different least squares algorithms in CDMA system are compared in [16] by ray tracing channel simulations. It is reported that the rapid convergence of the RLS - SQRLS makes them the most attractive choices in mobile communication applications. The blind algorithms generate the reference signal from the array output signal. The initialization of the weights is random and thus the algorithms may not converge to the desired solution.

2.3.4 Comparison of approaches

Figure 2.6 shows the simulated bit error rate (*BER*) v. signal-to-noise ratio (*SNR*) in a TDMA system for two adaptation strategies: the switched-beam antenna and the adaptive array using RLS algorithm with various numbers of antenna elements (*M*). Two users are served in the same traffic channel, and the angular user separation resolution of the adaptive array is 10°. [7]. The element spacing in the array is 0.5 λ, where λ is the signal free-space wavelength.

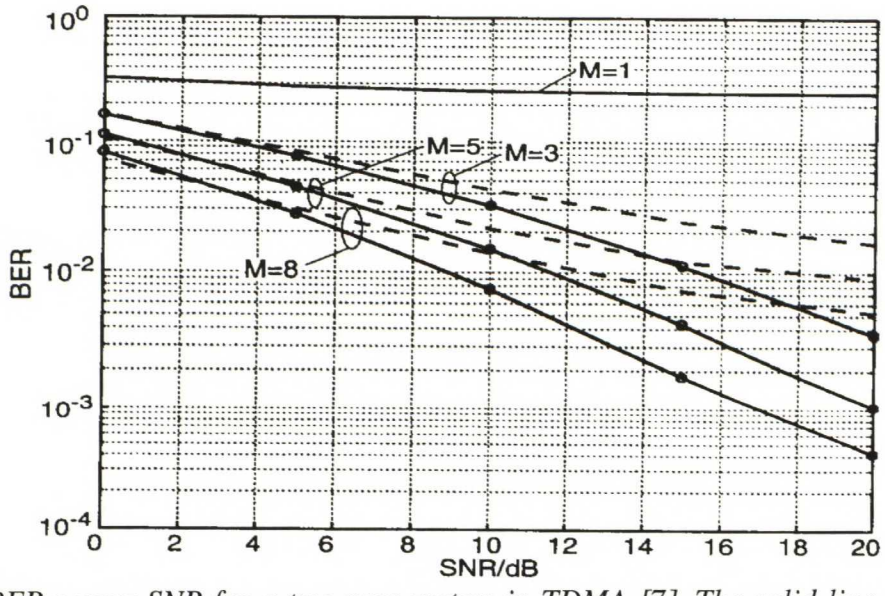

Figure 2.6. *BER versus SNR for a two-user system in TDMA [7]. The solid line represents the adaptive array, the dashed line the switched-beam antenna.*

The figure demonstrates that the performance of the switched-beam antenna is worse compared to the adaptive array, especially at high *SNR* conditions. This is due to fixed beams that can not point their maximum towards the wanted user and a zero in the interfering direction.

The advantages of adaptive arrays and SB-antennas in Digital European Cordless Telephone (DECT) system for indoor environments have been compared through ray tracing simulations in [4]. It is reported that the number of signal propagation paths are most often limited to just the direct path and the floor reflection path. In such conditions similar capacity increase was achieved with a switched sectored antenna as with an adaptive array. Thus, the amount of antenna complexity and price is dictated by the operating environment.

2.4 DIVERSITY SCHEMES FOR ADAPTIVE ARRAYS

Typically, there is no LOS between the transmitting and receiving antennas of a cellular system. The received signal is therefore a sum of multiple reflections of the original signal. Diversity in reception means receiving the same signal from different paths. These paths may vary in place, time, polarization, etc. The implementation of the diversity

scheme and the obtainable improvement in signal statistics relies on the availability of two or more independently fading signals with comparable mean signal levels [17]. In the following, some diversity schemes are considered that could be exploited by adaptive arrays.

2.4.1 Space diversity

Space diversity antennas are commonly used at base stations of cellular networks today. Reasonable improvement in received signal statistics can be achieved with the use of a horizontally spaced diversity antenna if the distance between the elements is about 5 λ in urban and at least 20 λ in suburban areas. This corresponds to correlation coefficient less than 0.6 which gives 8 dB improvement of carrier-to-noise ratio (*CNR*) with 99 % probability in a Rayleigh channel [18]. The presence of local scatterers degrades the performance.

Typically, in an antenna array the element separation is about one half of a wavelength, which is small considering space diversity. However, the distance between the end elements of a typical array is several wavelengths and with low coupling between antenna elements adaptive arrays could be able to provide space diversity. In addition, space diversity can be achieved by element spacing of 0.5 ... 1 λ whenever scatterers exist in the immediate vicinity of the BS antenna causing angular spreading of the signal such as in indoor environments [19,20].

2.4.2 Polarization diversity

The mobile systems usually use vertical linear polarization. When the transmitted wave propagates through the environment, it undergoes random changes in polarization. This is due to diffraction and scattering by objects. Also, the mobile antenna orientation depends on how the user is holding the handset. The changes in the plane of polarization result in fading of the received signal. According to [17] signals transmitted on two orthogonal polarizations exhibit uncorrelated fading statistics in the mobile radio environment.

If the antenna were capable of receiving two orthogonally polarized waves, it could take advantage of polarization diversity. The reception of any arbitrary polarization is possible, if the received signals from two antenna elements having different polarizations can be suitably weighted by a smart antenna. The applicability of polarization diversity leans on sufficiently small cross polarization discrimination (*XPD*) which describes the level difference of different polarization branches. Signal combining is not feasible if the difference in values exceeds 10 dB [21].

Because implementation of polarization diversity does not require physical separation of antennas, it is more easily implemented in antenna arrays than space diversity. By combining space and polarization diversity the physical size of the array may be reduced while maintaining the same overall number of diversity paths. It has been shown [22] that angular beam steering and polarization agility controls are independent. Because of the difference between the average powers received at the two polarizations, the polarization diversity is stated not to offer as large improvement in received signal as the other diversity schemes [18]. However, in mobile systems using hand-portable devices the mobile antenna orientation is random (often almost horizontal), and experiments have shown that in such situation polarization diversity may outperform space diversity [23].

2.4.3 Angular diversity

In some cases, e.g. if there are scatterers near the BS antenna, adaptive arrays can be used to provide angular diversity to the system. In such scheme, the multipath components of the same signal are received from different directions separated more from each other than the angular spread of one path. Greater part of the total radio energy can be collected and added together constructively in an optimal combiner [24]. This is an opposite point of view to the delay spread rejection presented in Sec. 2.2.1. The choice depends on the situation, mainly the environment.

2.4.4 Phase diversity

Except the amplitude patterns, adaptive arrays can form different phase patterns, even for nearly omnidirectional amplitude patterns. The channel fading is due to the multi-

path signal components canceling each other in the array input. By suitable phasing of the radiation pattern the antenna could prevent the signal cancellation in the array output. The phase diversity can be considered as a form of angular diversity.

2.4.5 Jitter diversity

Jitter diversity is a diversity scheme, where a beam, formed by an antenna array, is pointed at the main reception direction and then jittered around this direction to avoid deep angular fades [25]. The jittering is accomplished simply by changing the phasing of the array elements, which turns the beam. After detecting the direction of the maximum signal strength, the antenna starts to jitter around this maximum by turning the beam in the direction of the gradient to find the nearest local maximum. The global maximum has to be updated at some stage. In [25] diversity gains as high as 10 dB have been simulated with antenna beamwidth of 11.3° and 20° signal angular spread.

2.5 DIMENSIONS OF ADAPTIVITY

To describe an antenna radiation pattern in the spherical coordinate system, two angle variables are needed: azimuth and elevation. A phased antenna array can be adaptive in both or only one of the two dimensions. In a one-dimensional adaptive antenna the beam can be steered only in azimuth or elevation angle, whereas in a two-dimensional adaptive antenna beams can be pointed in any arbitrary angle in both directions.

In a cellular system with an adaptive array serving as a BS antenna, the need for dimensions of adaptivity is heavily dependent on the environment. In a typical macrocell in rural or suburban environment there are no scatterers near the antenna and most users can be assumed to be on ground level. In this case the main beam must be horizontal or slightly tilted downwards to serve users near the antenna. Azimuth angle adaptation alone is thus sufficient in this case.

In urban environment, especially when the BS antenna is situated under the roof-top level, the situation can be assumed different because of the reflectors near the antenna. The most crucial in this point of view is the indoor, or picocell environment where the radio channel is heavily affected by the echoes of the transmitted signal. Furthermore, in small urban cells the mobile is not always on the same vertical level with the BS (e.g. in high buildings). In such case two-dimensional adaptivity in the BS antenna might be useful.

2.6 ENVIRONMENT REQUIREMENTS

Different environments provide different propagation conditions. Therefore, the antenna applications will also become different. For example, beams must be wider in dense urban and indoor environments than rural because of the wider angular spread of the signal. Therefore it is expected that the isolation of the users and the capacity increase is not as good with small cells as it is with large cells [21]. Also different antenna geometries can be used to meet different environment requirements. Large macrocells benefit from arrays producing vertically narrow beams whereas wall-mounted planar arrays are appropriate for indoor picocells.

2.6.1 Rural and suburban environment

In rural environment the radiowave propagation is quite straight-forward. The most scatterers are close to the mobile resulting in fairly small path angular spread of the received signal, and well defined directions of arrival. In suburban environment with about one kilometer cell diameters the measured 3 dB signal path angular spread has been in the range of 5 - 6° [21]. This indicates that the optimum antenna 3 dB beamwidth in cellular SDMA applications is between 5 and 10° [21]. Narrower beams would improve the *SINR* and system efficiency only in very large rural cells. The angular spreading of the signal also suggests that adaptive null steering might not be efficient strategy in mobile communication systems. Placing nulls in the radiation pattern has been the basic type of operation in adaptive arrays applied in radars. In radar systems

LOS typically exists and the path angular spread is very small. In such case, a null in radiation pattern, although being narrow, is able to cancel the interfering signal. Producing multiple closely spaced nulls, in turn, is not feasible unless the number of array elements is very large (an N-element array can produce (N-1) nulls).

The high antenna gains due to arrays producing narrow beams can be exploited in lower density environments, where no scatterers exist near the antenna. In the case where co-channel interference in adjacent cells is not critical, high-gain downlink beams are useless. This is due to the available transmission power in the base station.

2.6.2 Urban and indoor environment

In [8] the measured gain improvement offered by multibeam BS antennas has been slightly better in light urban than in heavy urban environments. In a microcellular environment the closer proximity of scatterers cause increase in the angular spread of the signal. The measured indoor angular spread is reported to be up to 16° [21]. In [26] the ray tracing simulation technique is used to determine the effects of adaptive arrays to the signal delay spread at high bit rates (10 - 20 Mbit/s) in indoor environment. It is reported that substantial decrease in *BER* can be achieved by using adaptive arrays.

2.7 ERROR EFFECTS

As mentioned in Sec. 2.3.3, adaptive arrays based on the provision of a reference signal are insensitive to the imperfections in the array geometry or to the mutual coupling effects between array elements. Decorrelation effects due to frequency errors in the received signal can however cause problems in some systems [20]. This, of course, can not be compensated by antenna design.

In contrast, the implementation of beamforming techniques or adaptive algorithms based on directional information requires precise knowledge of the antenna properties. This kind of adaptive antennas are sensitive to the electromagnetic characteristics of the radiators. Changes in those characteristics due to environmental effects can cause severe

deterioration in the antenna operation. Therefore, the possible effects have to be predicted and prevented. The nonideal radio environment is another source of uncertainty if transmission is considered in beamforming applications. The next two sections describe the possible error effects related to such systems.

2.7.1 Nonidealities in array

The simulated capacity improvement achieved by adaptive antennas has shown substantial decrease for beam mispointing exceeding 2° [12]. The beam mispointing can be caused by coupling between the elements or by scatterers in the immediate vicinity of the antenna. The effects of the surroundings of the BS should be minimized and the antenna should be calibrated in its mounting place if close proximity scatterers exist.

Base station antennas are often used in places exposed to different weather conditions, which has to be taken into account in the design of the antennas. If a radome is needed, it must not perturb the radiation pattern. If large microstrip arrays are used, the thermal expansion effect due to heating in direct sunlight has to be considered. Changes in the array dimensions can affect the frequency response as well as the directional response of the array.

2.7.2 Nonidealities in radio environment

The operating environment of a BS antenna hardly ever completely corresponds to free propagation conditions. This means that the real antenna radiation pattern differs significantly from the theoretical pattern, or the pattern measured in laboratory conditions. For example the sidelobe levels of the antennas in a reflection-free environment experience substantial increase when the antenna is brought to operate in a typical cellular radio environment. The measured effective sidelobe levels in suburban environments have been as poor as -10 dB [21]. The effective antenna gain also depends on the environment. For wide angular spreads narrow high-gain beams reject part of the desired signal. Thus, in harsh environment, the performance of the antenna is not dictated solely by the antenna design.

3 Antenna arrays

In point-to-point communication applications (radio links), single antenna elements do not often provide required directivity and gain values. One convenient method to achieve narrow beams and high gains is to use an array composed of several antenna elements. This approach is similar to constructing an antenna with a large aperture. If the elements are uniformly distributed at the aperture and excited in phase, the result is a narrow directive beam perpendicular to the aperture surface. In theory, the beam can be made as narrow as necessary by increasing the size of the array. The radiation properties of the element may be simple, because the operation is based on the array effect.

A very important characteristic of array antennas is that beams and nulls can be created in arbitrary directions by suitable weighting of the element signals. Also, optimal radiation patterns with e.g. lower sidelobes may be obtained through pattern synthesis. These particular properties are the ones that form the basis of beamforming antennas and adaptive arrays.

3.1 Introduction to antenna arrays

The traditional concept of an antenna array is defined as a system of identical and identically oriented antennas with similar current distributions [27]. It can be shown that the radiated field from such an array may be written as a product of two terms

$$F(\theta,\phi) = f(\theta,\phi) \cdot e(\theta,\phi) \tag{3.1}$$

where $f(\theta,\phi)$ is the array factor, $e(\theta,\phi)$ is the element pattern, and $F(\theta,\phi)$ is the total radiation pattern of the array. The element pattern is the radiation pattern of one element i.e. the far field it radiates. The array factor depends on the geometrical distribution and the excitation of the elements. If the element pattern is broad, the array factor defines the radiation characteristics of the array. Similarly, narrow element patterns contribute to high gain and low sidelobes, if wide scanning is not required. Equation (3.1) is also known as the principle of pattern multiplication. It does not exactly hold true in practice, because the radiation pattern of a single antenna element changes from its isolated value when surrounded by other elements. Therefore, the elements near the edges of an array have different radiation patterns than the center elements. The reason for this is the mutual coupling between the elements.

Based on the definition above, the elements of an array can be specified by two quantities: the position from a reference element placed at the origin and the excitation amplitude and phase relative to the reference element. The array factor of an arbitrary antenna array can be written as [28]:

$$f(\boldsymbol{u_r}) = \sum_{n=1}^{N} a_n e^{jk\boldsymbol{u_r}\cdot\boldsymbol{r_n}} \tag{3.2}$$

$$k = \frac{2\pi}{\lambda} \tag{3.3}$$

where k is wave number, λ is free-space wavelength, a_n is complex excitation coefficient of n^{th} element, $\boldsymbol{r_n}$ is position vector of the element from the origin, and $\boldsymbol{u_r}$ is unit vector pointing to the radiation direction.

If the orientation of the element currents is not similar, the concept of the array does not hold. The array factor and the element pattern of such quasi-arrays [27] are not separable. However, in the case of adaptive arrays employing reference signal based algo-

rithms (see Sec. 2.3.3) the approach differs from that of traditional arrays, and such antennas are possible candidates for the implementation.

3.1.1 Basic antenna array parameters

Some of the definitions commonly used with antenna arrays are presented briefly in the following. Most of them are defined in terms of transmitting antennas, but they are applicable to receiving antennas as well by reciprocity.

Main beam

The main beam of the radiation pattern of an antenna is the lobe containing the direction of maximum radiation power.

Sidelobes

Sidelobes are the lobes in an array radiation pattern pointing towards other directions than the main direction. For example, the level of the first sidelobes (next to the main beam) of a linear array with uniform amplitude illumination is about 13 dB below the peak of the main beam.

Grating lobe

Grating lobes are extra main beams in the radiation pattern of an array. They are caused by too large element spacing, so that several directions exist in which the fields radiated by different elements sum in phase.

Beamwidth

The beamwidth of an array is the angular width of the main beam in its radiation pattern. The half-power beamwidth (*HPBW*), or 3 dB beamwidth is measured between the points on the main beam that are 3 dB below the peak of the beam. The beamwidth depends on the largest dimension of the antenna aperture.

Directive gain

The directive gain is defined as the ratio of the radiation intensity per unit solid angle $W(\theta,\phi)$ in a particular angular direction in space to the total radiation power of the antenna

$$D(\theta,\phi) = 4\pi \frac{W(\theta,\phi)}{P_{rad}} = \frac{4\pi W(\theta,\phi)}{\iint_{4\pi} W(\theta,\phi)\mathrm{d}\Omega} \tag{3.4}$$

Directivity

Directivity is the maximum value of directive gain.

Antenna gain

The gain of an antenna is the ratio of the radiation intensity per unit solid angle to the total input power to the antenna. It is the product of the directive gain and antenna efficiency.

3.1.2 Element spacing

An antenna array can be considered as a sampled aperture. When an array is illuminated by a source, the field at the aperture is sampled at the element locations. For this reason, the spacing of the array elements plays a significant role in the array theory.

The Nyquist criterion states that at least two samples per wavelength must be taken to correctly 'record' the radiation in all directions (assuming that the mirror beam is suppressed, refer to Sec. 3.2.1). If the element spacing d is larger than $\lambda/2$, grating lobes begin to rise due to spatial aliasing. If the spacing exceeds one wavelength, the pattern becomes ambiguous because the grating lobes are as high as the main beam. In such situation several directions exist from where the waves sum in phase at the elements. The grating lobes occur to angles θ_p such that

$$\sin\theta_p = \sin\theta_0 + \frac{p\lambda}{d} \quad , \quad p = \pm(1,2,\ldots) \tag{3.5}$$

for values of p that define an angle with real sine [29], when θ_0 is the main beam direction.

If the antenna operates at a limited field of view, the spacing can be chosen larger than $\lambda/2$ to cover larger aperture and thus obtain narrower beam. Element spacing smaller than $\lambda/2$ wastes elements because smaller aperture is covered with the same number of elements. It also contributes to coupling between the elements. However, according to [29], the impedance mismatch due to array scanning is smaller for small element spacing (see Sec. 3.5.2). The usual choice for the spacing is $\lambda/2$. The spatial aliasing phenomenon occurs when the operating frequency increases; the wavelength decreases and the distance between elements relative to wavelength increases. This limits the bandwidth of the array. Figure 3.1 shows the spatial aliasing in the array factor of an 8-element linear array. The narrower beam in Fig. 3.1 (b) is due to the larger aperture.

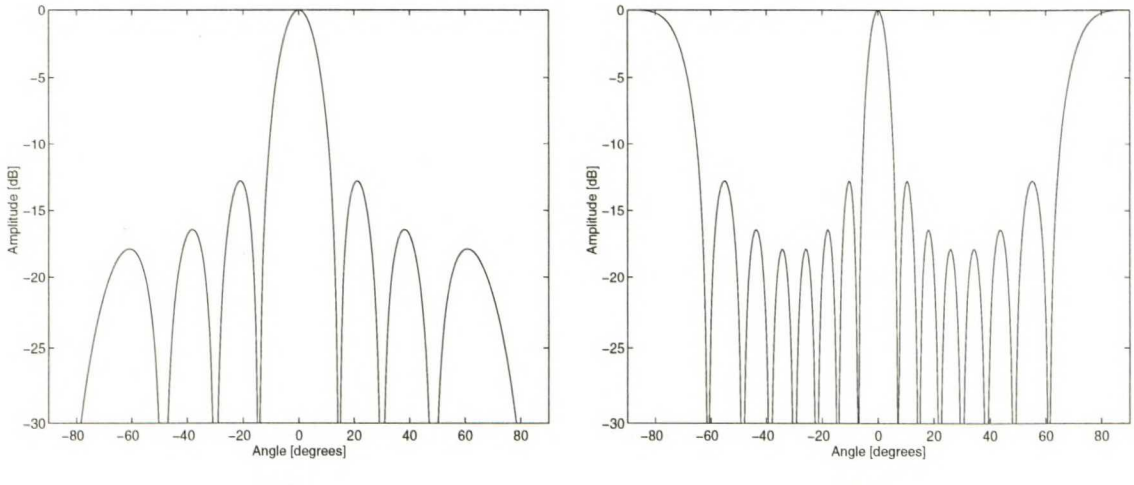

Figure 3.1. *Effect of element spacing in the array factor of 8-element linear array. (a) d = $\lambda/2$. (b) d = λ.*

The grating lobes due to spatial aliasing limit the interference rejection capability of macrocell antennas with large field of view. Instead, in micro- or picocells, the BS location may be such that only small angular sectors are of interest and grating lobes appearing in wider angles can be suppressed e.g. by choosing a suitable element pattern. The effect of the grating lobes depends also on the operational target of the array, e.g. interference rejection or delay spread reduction.

The effect of the element spacing in the array on the performance of adaptive arrays has been studied in [30]. It is reported that the user separation potential of adaptive antennas increases along with increasing element spacing in the array, if the number of elements is kept constant. This is due to the narrower beam. Furthermore, it is stated that the disadvantage of spatial aliasing in the pattern is outweighed by the narrower beam.

In [26] a ray tracing simulation of circular adaptive arrays inside an office building is conducted, and the effects of the circle radius on the performance of arrays for intersymbol interference reduction have been studied. The results indicate that the presence of grating lobes does not affect the delay spread rejection performance. If the radius is 0.5 λ, increasing the element number from 4 to 16 does not significantly improve the *BER*. This is due to the small aperture incapable of providing a narrow beam. If the radius is increased to 2 λ, the improvement is remarkable. One can assume that this is caused by the small probability of the grating lobes to appear in the random directions of the echoes of the signals.

3.2 ARRAY GEOMETRIES

Different antenna array geometries result in different radiation characteristics, and when scanning is considered, required scan direction characteristics can be obtained by suitable design geometry. A few common array geometries are presented in the following sections.

3.2.1 Linear array

The simplest array configuration is an array consisting of N elements placed along a line with equal spacing d from each other. The first element is placed at the origin. The geometry of this configuration is shown in Figure 3.2.

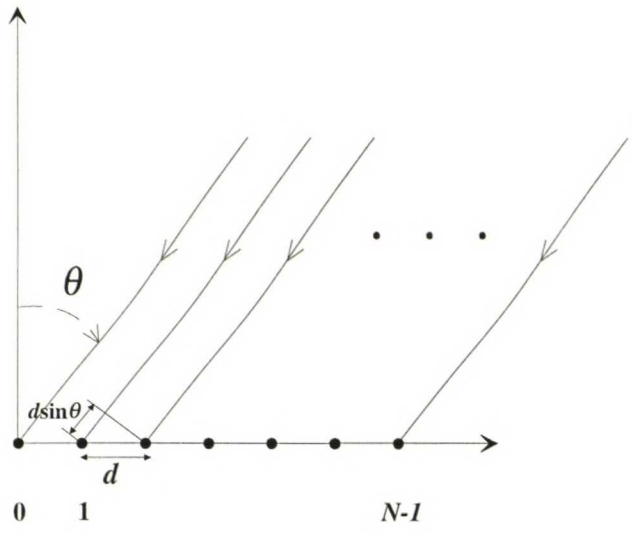

Figure 3.2. *Uniformly spaced linear array.*

If a plane wave arrives at the array from angle θ (> 0) with respect to the array normal, it reaches element $n + 1$ sooner than element n. This is because the differential distance along the two ray paths is $d\sin\theta$ (see Fig. 3.2). If the phase of the first element is set to zero, the phase of the n^{th} element is

$$\delta_n = nkd\sin\theta \tag{3.6}$$

If the elements are omnidirectional and each element signal is weighted with complex coefficient w_n, the resulting signals are

$$s_n = w_n e^{j\delta_n} = w_n e^{jnkd\sin\theta} \tag{3.7}$$

The array factor of the array is written as the sum of the element signals

$$f(\theta) = \sum_{n=0}^{N-1} w_n e^{jnkd\sin\theta} \tag{3.8}$$

If the weights of the elements are chosen as

$$w_n = a_n e^{jn\alpha} \tag{3.9}$$

where a_n is the real amplitude coefficient and $\alpha = -kd\sin\theta$ is the phase difference between adjacent elements, the array factor will become

$$f(\theta) = \sum_{n=0}^{N-1} a_n e^{jn(kd\sin\theta+\alpha)} \tag{3.10}$$

From (3.10) it can be seen that by setting the phase shift to $\alpha = -kd\sin\theta_0$, the maximum of the array factor is steered towards angle θ_0. The array factor of the linear array depends in space only on θ thus being rotationally symmetric about the array axis. If the elements are omnidirectional, a ground screen can be used to eliminate the mirror image beam.

In the maximum direction the waves from different antenna elements sum in phase. Similarly, no energy is radiated towards the directions where the waves cancel each other, called pattern nulls. If α is set to zero the main beam will occur at the direction perpendicular to the array axis ($\theta = 0°$) called *broadside* direction. Setting $\alpha = kd$ alternatively turns the main beam parallel to the array axis ($\theta = 90°$) called *end-fire* direction. Figure 3.3 presents two examples of array factors for linear arrays. The pattern is shown only for values of θ from -90° to 90°. If the elements were isotropic, the same pattern would occur also in the other half-space.

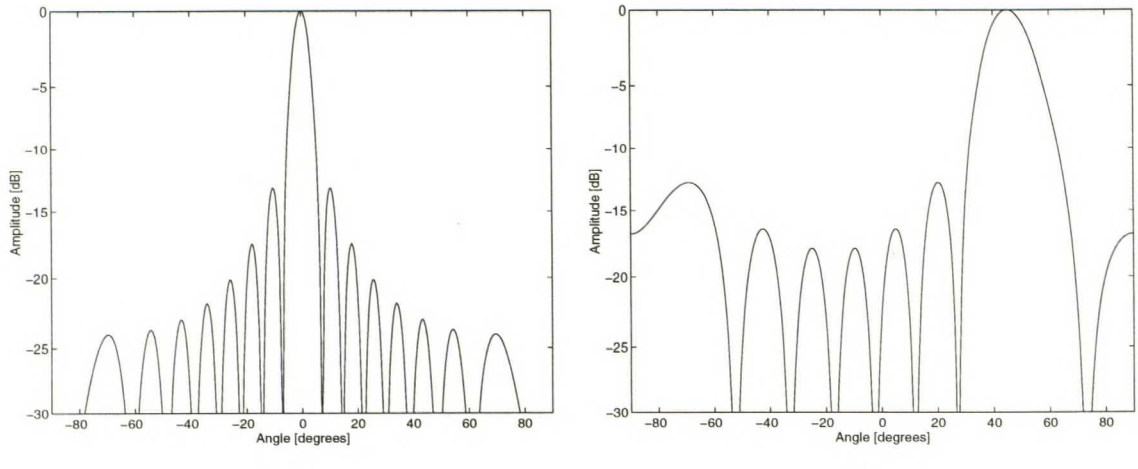

(a) *(b)*

Figure 3.3. *Examples of array factors of linear arrays ($d=\lambda/2$). (a) $N = 16$, $\theta_0 = 0°$. (b) $N = 8$, $\theta_0 = 45°$.*

Figure 3.3 shows that - with the same spacing between elements - additional elements make the main beam narrower. This is due to the increase of the aperture. Narrow beam means high directivity and gain. The beamwidth also determines the angular resolution of the adaptive array and thus its capability to separate spatially the users in the same traffic channel.

The minimum beamwidth of a linear array is achieved with uniform amplitude and phase illumination (beam steered to broadside). In this case, the 3 dB beamwidth in radians is

$$HPBW_{\min} = \frac{0{,}886\lambda}{L} \tag{3.11}$$

where L is length of the array [29]. The main beam widens from its broadside value when scanned to end-fire due to the visible aperture diminishing. For an 8-element array with $\theta_0 = 45°$ (Fig. 3.3 (b)) the 3 dB beamwidth is about 18.5°, while in broadside it is about 13°. The array directivity of a broadside linear array is approximately

$$D = \frac{2Nd}{\lambda} \tag{3.12}$$

[28]. If $d = \lambda/2$ the directivity is simply N, and does not change with the array scan angle [28]. This is also the maximum directivity achieved with any illumination (except for superdirectivity, see Sec. 3.4.4). The disadvantage of the uniform amplitude illumination is the high resulting sidelobe level, which is about 13 dB below the peak of the main beam (see Fig. 3.3).

By using more complex excitation coefficients different radiation patterns can be obtained for the same array. Different methods are developed to synthesize radiation patterns with low sidelobes or nulls pointing at certain directions. These are e.g. Dolph-Chebyshev's, Schelkunoff's, and Taylor's method [29,31]. Desired properties are narrow beam, low sidelobe level, and small number of elements. These conditions are,

however, contradictory, and if the pattern is optimized with respect to one parameter, the other parameters will suffer.

The Chebyshev amplitude illumination provides the lowest sidelobes for a given maximum beamwidth and given number of elements, or vice versa. Figure 3.4 shows the array factor of an 8-element linear array ($d = \lambda/2$) with uniform phase illumination and Chebyshev amplitude weighting to achieve -30 dB sidelobes. The 3 dB beamwidth is increased to 16° from the 13° obtained with uniform illumination.

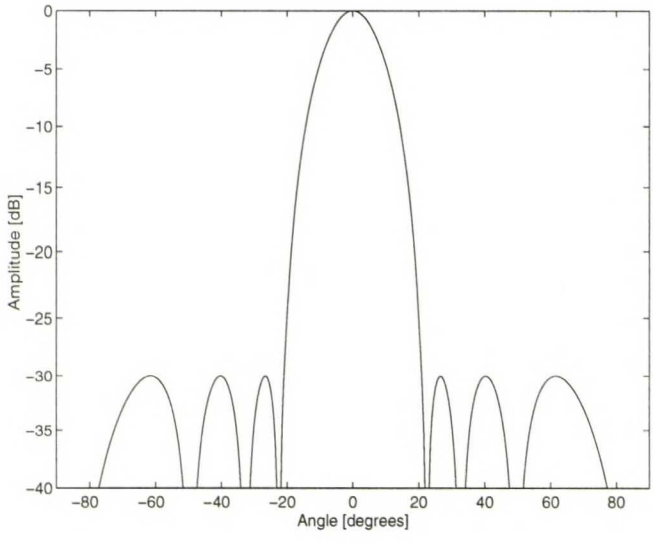

Figure 3.4. *Array factor of 8-element linear array with Chebyshev weighting for -30 dB sidelobes.*

3.2.2 Planar array

The two-dimensional planar array consists of radiators arranged on a plane. On each side of the array plane, the radiation pattern has one beam which can be steered towards any angle (θ_0, ϕ_0) in the half space. Figure 3.5 shows the rectangular array, which is a linear array of elements, each of which is a linear array.

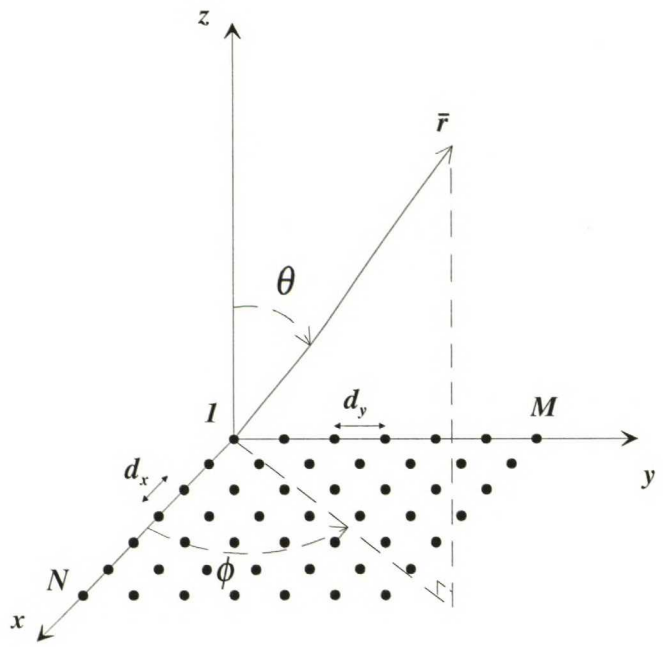

Figure 3.5. *Geometry of rectangular array.*

According to the principle of pattern multiplication, the element factor is independent of the array factor, which means that the element may be an array as well. Thus, the array factor of the rectangular array can be written as the product of the array factors of two linear arrays

$$f(\theta,\phi) = f_1(u) \cdot f_2(v) \tag{3.13}$$

where

$$f_1(u) = \sum_{n=0}^{N-1} a_n e^{j(nkd_x \sin u + n\alpha)} \qquad u = \sin\theta\cos\phi \tag{3.14}$$

and

$$f_2(v) = \sum_{m=0}^{M-1} b_m e^{j(mkd_y \sin v + m\beta)} \qquad v = \sin\theta\sin\phi \tag{3.15}$$

[32]. N and M represent the numbers of elements in each dimension of the array (see Fig. 3.5). d_x and d_y are the corresponding element spacings. Coefficients $a_n e^{jn\alpha}$ and $b_m e^{jm\beta}$ are the complex weights of the element signals. To steer the main beam towards the direction (θ_0, ϕ_0), the element phases have to be $\alpha = -kd_x \sin u_0$ and $\beta = kd_y \sin v_0$. If scanning is not required in both dimensions, the linear arrays at the other dimension may

be excited in phase. The result is a higher gain compared to the case of a linear array of single elements.

For most practical illuminations the directivity of a planar array can be written as [33]

$$D = \frac{\pi^2}{\Omega_A\left(\text{rads}^2\right)} = \frac{32{,}400}{\Omega_A\left(\text{degrees}^2\right)} \tag{3.16}$$

where Ω_A is a beam solid angle defined as the product of the half-power beamwidth in the *yz*-plane (Θ_{3dB}) and in the *xy*-plane (Ψ_{3dB}) [33]

$$\Omega_A = \Theta_{3dB} \cdot \Psi_{3dB} \tag{3.17}$$

The beamwidths in both dimensions are given approximately as

$$\Theta_{3dB} = \sqrt{\frac{1}{\cos^2\theta_0\left[\Theta_{x0}{}^{-2}\cos^2\phi_0 + \Theta_{y0}{}^{-2}\sin^2\phi_0\right]}} \tag{3.18}$$

and

$$\Psi_{3dB} = \sqrt{\frac{1}{\Theta_{x0}{}^{-2}\sin^2\phi_0 + \Theta_{y0}{}^{-2}\cos^2\phi_0}} \tag{3.19}$$

where Θ_{x0} and Θ_{y0} represent the half-power beamwidths of the linear arrays along *x*- and *y*-axis (see Fig. 3.5) scanned to broadside [33].

The radiation pattern of a broadside rectangular array of 8 × 8 elements with $d_x = d_y = \lambda/2$ is given in Figure 3.6.

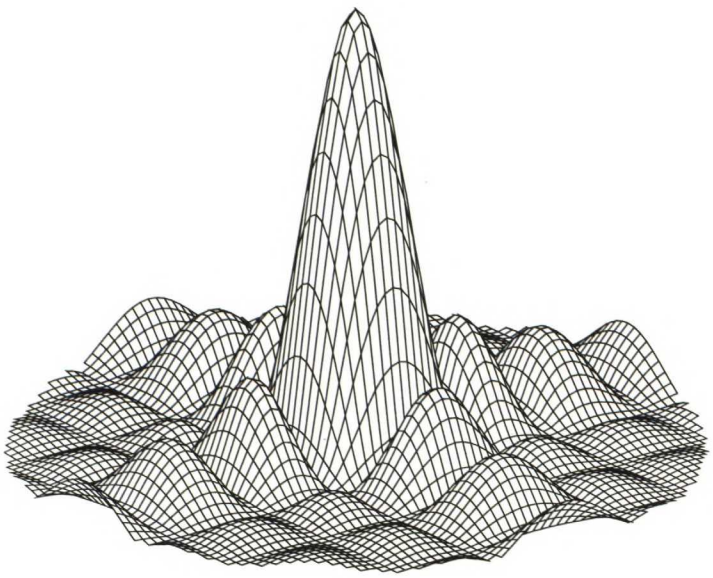

Figure 3.6. *Three-dimensional radiation pattern of 8 × 8 rectangular array with $d_x = d_y = \lambda/2$. Angle θ is the distance from origin in xy-plane, ϕ circles around the z-axis (see Fig. 3.5).*

3.2.3 Circular array

One interesting form of planar array configuration is the circular, or ring array, in which the elements are placed along the circumference of a circle. Figure 3.7 shows the geometry of a circular array with evenly spaced elements on *xy*-plane.

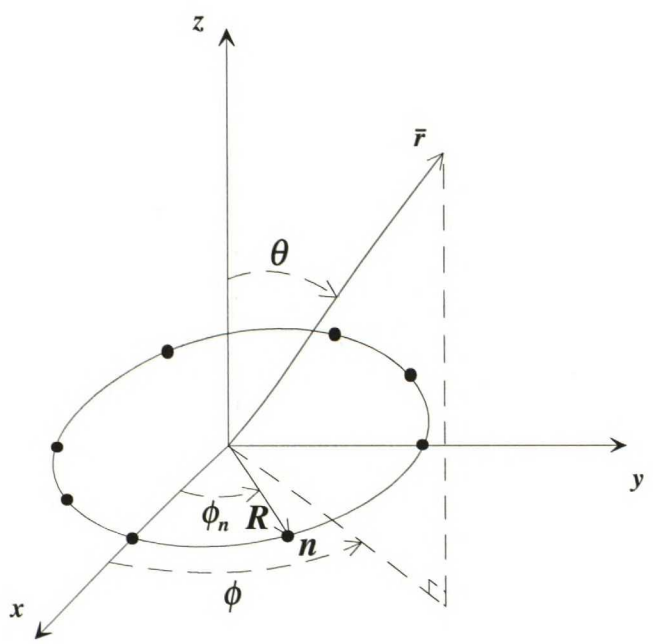

Figure 3.7. *Geometry of circular array.*

The array factor for a circular array of N equally spaced elements is given as [32]

$$f(\theta,\phi) = \sum_{n=0}^{N-1} a_n e^{j\left[\alpha_n - kR\cos(\phi-\phi_n)\sin\theta\right]} \tag{3.20}$$

where $a_n e^{j\alpha_n}$ is the complex weight of the n^{th} element, ϕ_n is the azimuth angle of the n^{th} element, and R is the radius of the circle. To have the main beam directed at the angle (θ_0, ϕ_0), the phases of the weights must be chosen as

$$\alpha_n = kR\cos(\phi_0 - \phi_n)\sin\theta_0 \tag{3.21}$$

Pattern synthesis for circular arrays is given e.g. in [34,35]. If beam steering is required only in the horizontal plane, the gain can be increased by using vertical linear arrays as array elements.

Figure 3.8 shows the array pattern of a circular array of 24 elements with the main beam steered towards $\theta_0 = 0$. The diameter of the circle is 3.5λ..

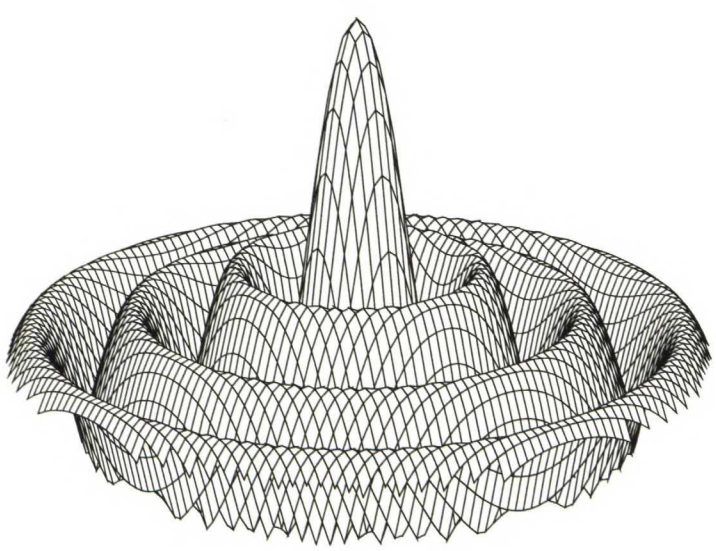

Figure 3.8. *Three-dimensional radiation pattern of 24-element circular array, $R=1.75\lambda$.*

In BS antenna applications, the principal plane radiation pattern ($\theta = 90°$) is of interest. Figure 3.9 presents the horizontal radiation pattern of a 24-element circular array with $R = 1.75\lambda$. Beam is steered towards $\phi_0 = 0$. Only one half of the pattern is shown.

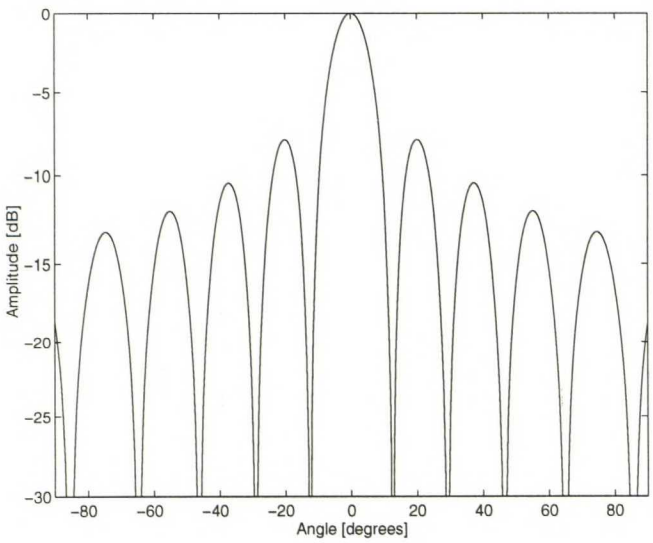

Figure 3.9. *Horizontal radiation pattern of 24-element circular array with $R = 1.75\lambda$.*

One drawback of the circular array - its high sidelobe level - shows clearly in Fig. 3.9. For uniform amplitude illumination and equal element spacing the lowest achievable level is about -8 dB compared to the main beam [32]. One advantage is, on the other hand, that because of the symmetry, the beamwidth does not change with azimuth scanning, like is the case with linear arrays. Linear and planar arrays are usually limited to scan angles of about ±70° from broadside because of gain reductions and aperture mismatch losses [36].

When adaptive BS arrays are considered, there is a choice to be made between a circular array and a sectored structure of several linear arrays. Table 3.1 compares the properties of both configurations with the same number of elements. The sectored antenna consists of three linear arrays with $d = \lambda/2$. The diameter of the circle is the same as the length of the linear array. Both have uniform amplitude illumination.

Table 3.1. *Comparison of two base station array configurations.*

	24-element circular array	**Sectored configuration of three 8-element linear arrays**
Largest dimension	3.5 λ	3.5 λ
Minimum 3 dB beamwidth	12°	13°
Maximum 3 dB beamwidth	12°	29°
Maximum sidelobe level	-7.9 dB	-13.5 dB
Merits & Drawbacks	**+ beamwidth does not change with scan angle** **+ no switching network** **- high side lobes**	**- beam broadens with scan angle** **- requires switching** **+ lower side lobes**

For uniform illumination, the circular array has narrower mean beamwidth, but higher sidelobes. The sidelobes can be lowered by tapering the amplitude, which widens the beam. The sectored array suffers from the beam widening with increasing scan angle (the maximum beamwidth corresponds to ±60° scan). It also requires a switching network to correctly perform the 'handover' to the adjacent array, when the beam is steered beyond the limit. One considerable limitation of the circular array is, that if the elements are omnidirectional, the array bandwidth is very narrow. This is due to cancellation effects between the elements at opposite sides of the ring [29]. The bandwidth criterion is approximately

$$\frac{\Delta f}{f_0} = \frac{\lambda}{8R} \tag{3.22}$$

[29]. This leads to only 7 % bandwidth for the circular array of Table 3.1. On the other hand, a circular array of omnidirectional elements provides vertical directivity not achieved with linear arrays.

It should be noted, that in Table 3.1 the antenna elements are presumed isotropic, and the properties will become different for real elements. For example, with wide scan angles, the gain of a linear array is limited by the element pattern. Therefore, the choice of the element depends on the array geometry.

3.2.4 Thinned arrays

With thinned arrays the number of elements required to achieve wanted resolution is minimized by removing elements from the array. The subject of thinned arrays is traditionally associated with radio astronomy applications. In [37], a 5-element thinned linear array for earth remote sensing is presented. The elements are spaced at certain integer multiplies of $\lambda/2$ so that every half-wavelength spacing up to 4 λ is available. Figure 3.10 presents the configuration.

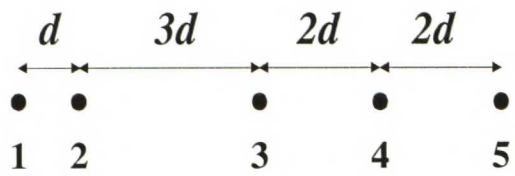

Figure 3.10. *5-element thinned linear array, d=λ/2.*

By cross-correlating all ten possible pairs of antenna signals one is able to get the same resolution as if the array was filled with 9 elements spaced $\lambda/2$ apart. This technique is known as aperture synthesis, and an array employing it is a minimum redundancy array (MRA) [38]. The savings in system complexity and costs compared to filled array are evident, because of the fewer required receiver front-ends.

Examples of using thinned adaptive arrays in CDMA system are proposed in [39,40]. The concept is based on replacing some of the antenna elements by virtual elements to get larger aperture for a given number of elements. Virtual elements are needed to avoid spatial aliasing. The virtual element signals are estimated by appropriate signal processing methods. The increased element spacing results in reduced coupling effects and narrowed beams due to the wider antenna aperture. Also, according to [19], whenever scatterers exist in the immediate vicinity of the base station antenna such as in the indoor environments, the element spacing farther than $\lambda/2$ provides spatial diversity to combat fading.

3.2.5 Other geometries

In addition to the previous, some other array configurations worth mentioning are the three-dimensional conformal arrays, namely cylindrical, conical, and spherical array [36]. With these, the antenna elements are positioned on a 3D surface offering additional options in pattern shaping.

3.3 ANTENNA ELEMENTS

If the antenna elements were isotropic, the radiation pattern of the array would coincide with the pattern defined by the array factor. However, isotropic antenna elements do not exist in real life. Instead, all practical antenna elements have nonuniform radiation patterns that affect the pattern of an array composed of the elements. The wire elements including dipoles and monopoles are the most common used types in applications of wireless communications. The attractive properties of printed elements are making them more and more popular. Horns and waveguide slots are traditionally the most common used elements in military applications of phased radar arrays. They would however become impractically big at 2 GHz frequencies, which are considered in this work.

3.3.1 Dipoles and monopoles

The $\lambda/2$-dipole and $\lambda/4$-monopole are typical antenna elements. The radiation pattern of a vertical dipole or monopole is omnidirectional in horizontal plane (H-plane). The pattern of the $\lambda/2$-dipole has a shape of a donut, i.e. its cross-section has two symmetrical beams in the vertical plane. The $\lambda/2$-dipole has 78° 3 dB beamwidth, and 2.1 dB directivity. The $\lambda/4$-monopole over an infinitely large perfectly conducting ground plane has similar radiation characteristics than a $\lambda/2$-dipole except for the missing lower half-space. The gain is 3 dB higher because of the ground plane. In practice the ground plane is not ideal and the beam is slightly tilted upwards from horizontal direction. This must be considered in the design of arrays. In base stations of small cells monopole arrays might be placed upside-down to exploit the pattern tilting. The $\lambda/4$-monopole has 5.1 dB

theoretical directivity and its E-plane beamwidth is one half of the beamwidth of a corresponding dipole.

3.3.2 Printed elements

If the number of array elements is large, printed antenna elements are the most convenient at 2 GHz frequency. The printed elements have many attractive properties. They are planar, simple, lightweight, low cost, easy to manufacture and easily integrated to other circuitry. Dipoles and monopoles have traditionally been constructed of metal wires. At low frequencies this is the only reasonable way to build elements that are of the order of the wavelength. At higher frequencies, however, dipoles printed on substrate may be easier to manufacture. Also the balun required by the dipole can easily be implemented on the same substrate, as well as feed networks for arrays.

Another printed element is the microstrip patch, of which the most common types are the rectangular and circular patch. Though the many convenient properties, patches have some disadvantages. They are resonators and thus have narrow frequency bandwidths by nature. Recently, great effort has been made in order to develop patch structures with wider bandwidths [41,42]. Other drawbacks include poor polarization purity, low efficiency, and surface-wave excitation. The last is particularly harmful with adaptive arrays since it can cause blind spots at some scan angles. Patch antenna designs concentrating on surface-wave rejection are studied in [43]. The microstrip patch antenna has broad beam (*HPBW* of the order of 100° in H-plane and a little less in E-plane depending on the dimensions of the antenna). The radiation is mainly concentrated in the upper half-space only due to the ground plane under the patch. This affects the design of the array.

3.3.3 Arraying of elements

The array definition limits the geometry of an antenna array. The adaptive array, however, can be considered as a group of sensor elements rather than a conventional array. Polarization adaptivity, for example does not fit into the array definition because of the current orientation requirement. The geometry of arrays of this kind is limited merely by ones imagination. The element positioning and orienting in an array depend heavily on

the required radiating directions of the antenna. If, e.g. whole 360° azimuth scanning is required, a single linear array of patches is not suitable. Instead, a sectored configuration of three linear arrays placed on sides of a triangle might meet the specifications. One possible choice is also a cylindrical array of patches. It does not satisfy the array definition because the element patterns need to be rotated, but is a suitable candidate for an adaptive array application. Some array geometries using different elements are presented in Figs. 3.11 - 3.14.

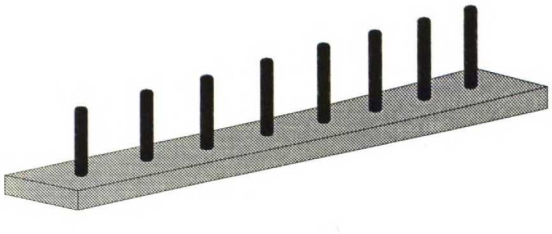

Figure 3.11. *Linear array of monopoles.*

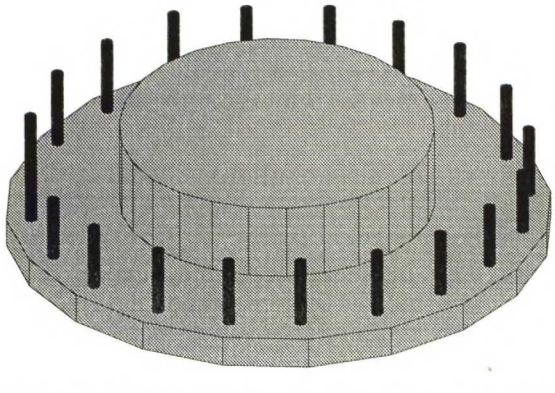

Figure 3.12. *Ring array of monopoles. Back plane is used to alleviate cancellation effects.*

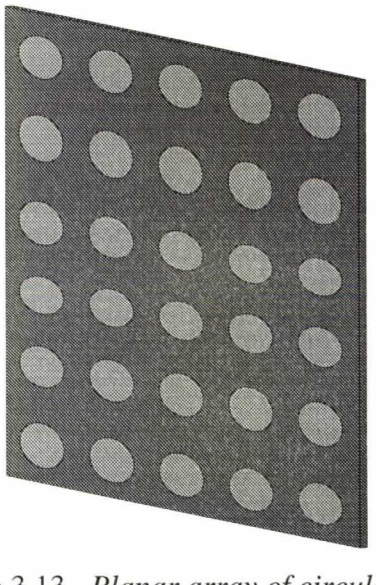

Figure 3.13. *Planar array of circular patches.*

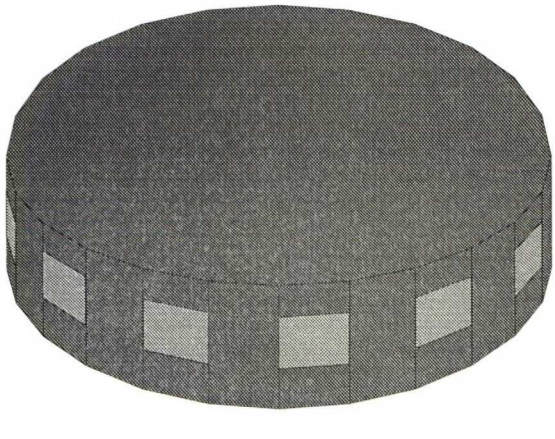

Figure 3.14. *Cylindrical array of rectangular patches.*

3.4 BEAMFORMING

3.4.1 Phased arrays

The radiation pattern of an antenna array depends on the weighting of the element signals. If the phase of the signal is changed, the main beam of the antenna is turned. Controlling also the amplitudes of the elements allows more sophisticated pattern control. Phased arrays have traditionally been used in radars. Compared to mechanical antenna rotation the phasing is a very useful method for tracking many moving targets. The beam can be pointed to a new direction and also widened or narrowed very fast. For the same reasons, scanned arrays are appropriate also for mobile communication systems. The concept is however far more complex because of the larger number of necessary beams and the difficult, ever changing propagation environment.

If the transmission and reception are on the same frequency, the signal weights for both directions are also the same. Radar arrays applying this property are called retrodirective arrays [44]. Most mobile systems, however, use FDD and can not thus exploit this property, because of the fading due to multipath propagation, which is frequency dependent. At least the signal weights obtained from received data have to be transformed to the transmission frequency. This requires accurate knowledge of the directional response of the array [45].

3.4.2 Analog beamforming

Analog beamforming means controlling of the element signals by passive devices: phase shifters, power dividers and attenuators. A beamforming network is required to produce one or multiple beams at the same time. Analog beamforming can be carried out either at RF or intermediate frequencies (IF). The latter requires a receiver behind each element, but losses in the beamforming network are less important. A beamforming network producing more than one beam is called a beamforming matrix, the best known type of which is the Butler matrix [29,46]. An $N \times N$ Butler matrix consists of N 90° hybrids and fixed phase shifters between the hybrids. It produces N orthogonal beams. At the crossover point of two beams the gain has reduced 3.9 dB, which is the minimum

achievable number with passive circuits. The price to be paid is the high sidelobe level (-13 dB). Figure 3.15 shows four orthogonal beams produced by a 4×4 Butler matrix.

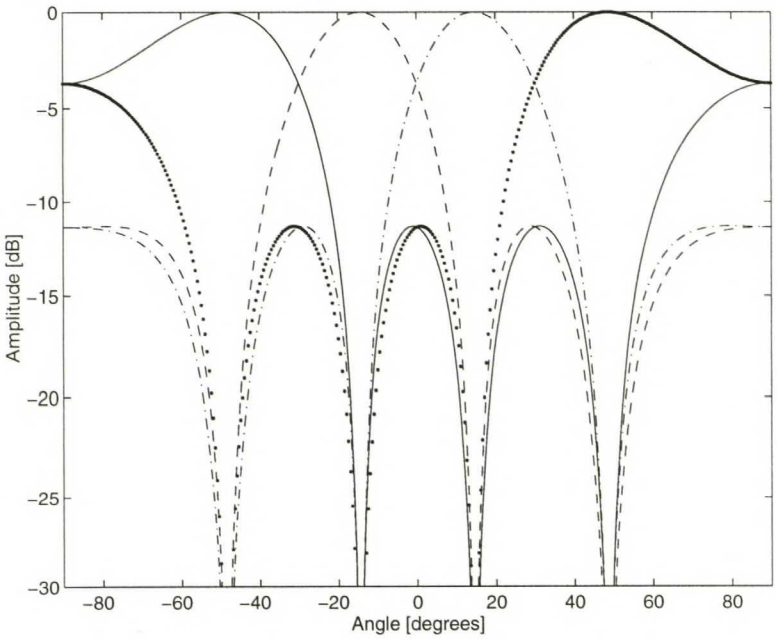

Figure 3.15. *Orthogonal beams produced by 4 ×4 Butler matrix (after [32]).*

If the phase shifts performed by the beamforming matrix are fixed, the antenna is of switched-beam type (see Sec. 2.3.1) and the radiation pattern consists of a set of beams with fixed pointing directions. Instead, if the beamforming network consists of (digitally) controlled phase shifters and attenuators, the pattern control is more flexible. Because the network operates at high frequencies, the error tolerances of the components are small, which may make them costly.

3.4.3 Digital beamforming

Digital beamforming (DBF) is based on the conversion of the RF signal from each antenna element into two binary baseband signals, representing the in-phase (I) and quadrature (Q) component channels. The conversion is accomplished using matched analog receivers and analog-to-digital converters (ADCs) in each element channel. The matching does not need to be performed with hardware, because the digital data can be corrected with pre-measured calibration data before the beamforming procedure.

After the conversion, the digital baseband signals contain as much of the information available at the antenna aperture as possible, depending on the number of bits in the ADCs. This information containing both amplitude and phase is then available for processing in the DBF computer. DBF allows more efficient control on the antenna parameters than conventional beamforming. In fact, a unique radiation pattern may be generated for each user. Figure 3.16 shows an example of uplink DBF implementation in a CDMA system.

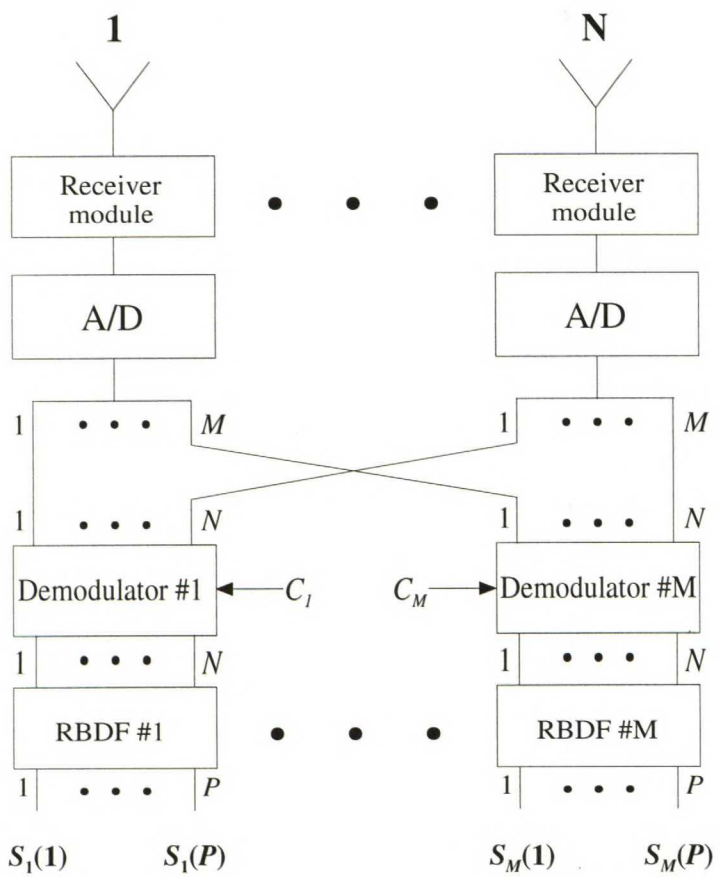

Figure 3.16. *Uplink DBF configuration for CDMA system (after [32]).*

After the A/D conversion the signals from N receivers are divided into M demodulators. The N demodulated signals are then fed to M DBF networks each producing P combinations corresponding to P beams in space. Unless superresolution is considered, the maximum value of P is equal to N. The number of simultaneous users can be up to $M \times P$ instead of M in the unadapted case.

Digital beamforming is a very attractive technique, but also costly. For this reason a trade-off should be made between the system efficiency and cost. A combination of analog and digital beamforming might be an optimum solution.

3.4.4 Superdirectivity

For arrays with element spacing greater than $\lambda/2$ the maximum directivity is achieved with uniform excitation (constant amplitude and linear phase). Superdirectivity is defined as directivity higher than that and applies to arrays with element spacing below $\lambda/2$. For example, uniform illumination results in directivity of N for spacing of both $\lambda/2$ and $\lambda/4$. However, at $\lambda/4$ spacing the optimum amplitude and phase excitation leads to directivity of N^2 [47]. Still, the optimum directivity is not achieved without any cost. The radiation quality factor Q_r increases exponentially when the directivity is higher than the conventional maximum. This leads to a very narrow bandwidth and extreme sensitivity to errors, as well as low efficiency, if optimum directivity is desired. Table 3.2 shows the element spacing, directivity and radiation quality factor for a linear array with $L = 2\ \lambda$ and designed sidelobe level of -20 dB.

Table 3.2. *Element spacing, directivity and radiation quality factor of linear array with $L = 2\ \lambda$. Designed sidelobe level is -20 dB (after [47]).*

N	d/λ	D	Q_r
5	0.500	4.69	1.7
7	0.333	5.18	7.0
9	0.250	6.21	$1.2 \cdot 10^6$
11	0.200	7.36	$5.8 \cdot 10^7$
13	0.167	8.54	$5.5 \cdot 10^{11}$

As can be seen in Table 3.2, some increase in directivity can be achieved with reasonable values of Q_r. In [48], a suboptimum constrained superdirective design is carried out to produce the lowest Q_r for a given directivity.

With digital beamforming superdirectivity could be employed to some extent, but the benefits in BS arrays can be questioned because the variable is the size of the array, not the number of antenna elements. Instead, if adaptive, or diversity antennas are considered in mobile equipment, the small element separation is essential.

3.4.5 Superresolution

The Rayleigh criterion states that two sources can not be resolved if their angular separation is less than the beamwidth of the receiving array. The *HPBW* of an 8-element linear array with $d = \lambda/2$ is about 13°. However, the same array can produce closely spaced nulls that are sharp in space. By calculating the inverse of the radiation pattern with suitable processing of the element signals one is able to generate two closely spaced beams [49]. Figure 3.17 presents the conventional beam pattern and the superresolution pattern for an 8-element linear array with $\lambda/2$ spacing. Two equally strong sources with *SNR* = 30 dB exist at 18° and 22°.

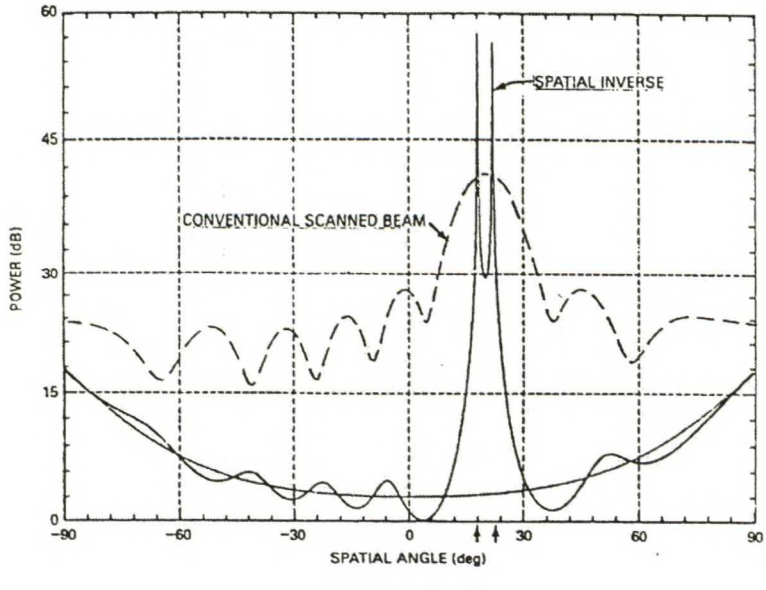

Figure 3.17. *Conventional scanned beam and superresolution pattern for 8-element linear array. Sources at 18° and 22° [49].*

The superresolution is sensitive to noise, which may be a significant limitation when mobile system applications are considered. The fundamental limit for superresolution with two equal sources can be written as [47]

$$SNR \approx \left(\frac{HPBW_{\text{Rayleigh}}}{HPBW_{\text{superresolution}}} \right) \tag{3.23}$$

3.5 LIMITATIONS AND EFFECTS OF ERRORS ON ADAPTIVE ARRAYS

3.5.1 Bandwidth

Because the main beam of a phased array is turned by changing the relative phases of the elements, it turns also when the frequency changes. This limits the bandwidth of phased arrays. The bandwidth of a linear array defined by the frequency limits where the gain towards the desired direction has reduced 3 dB, is

$$\frac{\Delta f}{f} = \frac{0.886\lambda}{L \sin\theta_0} \tag{3.24}$$

where L is the length of the linear array and θ_0 is the scan angle from broadside [29]. The bandwidth is smallest for large arrays and wide scan angles. For example, an array of length $L = 10\ \lambda$ gives a maximum scan angle of $\pm 62°$ for 10 % relative bandwidth.

The bandwidth of an array is limited also by the rise of grating lobes when the frequency increases. This is due to spatial aliasing presented in Sec. 3.1.2. Of course, also the bandwidths of single elements as well as other components of adaptive arrays: phase shifters, power dividers etc. affect the bandwidth of the system.

3.5.2 Mutual Coupling

The theory of phased array antennas is based on the pattern multiplication principle. This assumes that all elements have similar patterns in the array. In reality, the patterns of similar elements become different depending on the location of the element in the array, and the array scan angle. This is caused by the coupling of fields from other radiators in the array.

The mutual coupling of an N-element array can be presented through an $N \times N$ scattering matrix that relates the transmitted and reflected waves between each element pair. In an isolated case, the excitation of an element with amplitude a_m gives a value A_m for the amplitude of the electrical field in the element aperture. When the element is surrounded by other elements, the field depends also on the excitation of the other elements, and will become

$$A_m = \kappa\left(a_m + \sum S_{mn} a_n\right) \tag{3.25}$$

where S_{mn} is coupling coefficient between elements m and n [29]. Proportionality coefficient κ relates voltages to corresponding electrical fields. The coupling can be viewed from two alternative perspectives: the perspective of mutual impedances and the perspective of active element patterns. From the perspective of mutual impedances, the elements are considered as separate radiators with identical element patterns. Because of the mutual coupling, the impedances of the elements change when the array is scanned. In this case, the correct excitation amplitudes to obtain desired field amplitudes can be resolved from the measured scattering matrix. From the perspective of active element patterns, the complex radiation pattern of each element in the array environment is identified by exciting the element with all other elements terminated in matched loads. The scan-dependent radiation of the whole array can then be computed from the known patterns radiated by individual elements, assumed that the aperture fields have the same distributions on each element (single mode excitation) [29,50]. For most elements the higher order modes are negligible. The radiation of one element in a linear array can be expressed with the isolated element pattern $e_i(\theta)$ as

$$g_n(\theta) = e_i(\theta) \sum_{m=1}^{N} C_{mn} e^{jkmd \sin\theta} \tag{3.26}$$

where C_{mn} is coupling coefficient relating the signals at the n^{th} element to the signals at the m^{th} element [29]. The coefficients C_{mn} can be solved from the measured patterns.

If the mutual coupling is not compensated, it can lead to severe distortions in the radiation pattern. These distortions are angle and frequency dependent and consist of increased sidelobe levels, main beam squint, filled or shifted nulls, grating lobes and array blindness at some scan angles. Therefore, the mutual coupling should be measured and taken into account in order to correctly control the radiation of the array. The compensation of the pre-measured mutual impedances requires precise amplitude and phase control [29], but should be easily implemented with DBF.

The array blindness at some scan angles is due to surface wave excitation in dielectric materials, or other low loss modes of electric fields that may appear in periodic metal structures [29]. With suitable element phasing, the structure may be resonant causing the reflection coefficients to equal to unity, and the antenna radiates no energy. In [29] it is stated that scan blindness can be avoided by keeping the element spacing a few percent less than $\lambda/2$. This tunes the resonance off from the center frequency. Another means of scan blindness compensation is the usage of suitable dielectric radome, or metallic fences between the elements [29]. In the case of adaptive base station antennas, the scan blindness is a detrimental phenomenon, and has to be considered in the design of antennas. The use of two polarizations is also one possibility to avoid blind angles, since the blindness seldom occurs at the same angles in E-, and H-plane.

The effects of mutual coupling on the performance of an adaptive linear array of six $\lambda/2$-dipoles without coupling compensation have been studied in [51]. It is shown that the output *SINR* of an adaptive array depends on the angle of arrival of the desired signal in the presence of mutual coupling and decreases with increasing scan angle. The calculations indicate that the coupling degrades the performance of the array only for rather small interelement spacing. Compared to an array without mutual coupling, the drop in *SINR* is about 3 dB, when the interelement spacing is reduced to $\lambda/4$. For $\lambda/2$ spacing, the *SINR* is the same as without coupling. Beyond this point, the dependence of the *SINR* on the spacing is periodical so that the maximum drop is about 2 dB corresponding to element spacing of 1.1 λ.

3.5.3 Random errors in adaptive arrays

The theoretical antenna characteristics are not valid with practical system realizations. This is due to the finite accuracy of the weighting coefficients and the element positions. The root-mean-square (rms) error of the signal can be written in terms of its amplitude and phase error

$$\sigma = \sqrt{\sigma_a + \sigma_p} \tag{3.27}$$

where σ_a is rms amplitude error and σ_p is rms phase error. The effects of rms amplitude and phase errors on the properties of large two-dimensional arrays are presented in [52].

Main beam direction

The error in the main beam direction of an N-element array is [52]

$$\frac{\Delta}{HPBW} = \sqrt{\frac{3}{N}}\frac{\sigma}{0.88 \cdot \pi} \tag{3.28}$$

where the rms mispointing angle Δ and the half-power beamwidth are in radians.

Sidelobe level

The sidelobe level (SLL) in dB is written as [52]

$$SLL = 20\log_{10}\left(10^{\frac{SLL_0}{20}} + \frac{2 \cdot \sigma}{\sqrt{\varepsilon_T \cdot N}}\right) \tag{3.29}$$

where SLL_0 is the sidelobe level of the array without errors, and ε_T is taper efficiency defined as [29]

$$\varepsilon_T = \frac{\left|\sum a_n\right|^2}{N\sum\left|a_n\right|^2} \tag{3.30}$$

Directivity

The directivity in presence of amplitude and phase errors is [52]

$$\frac{D}{D_0} = \frac{1}{1 + \frac{3\pi}{4} \cdot \left(\frac{d}{\lambda}\right)^2 \cdot \sigma^2} \tag{3.31}$$

where D_0 is the directivity of the array without errors, and d is element spacing.

The error effects on several antenna parameters are studied in [21]. The simulations were made for linear arrays of 8,10 and 16 elements with $d = \lambda/2$. The errors in different elements were assumed mutually independent and uniformly distributed. The results indicate that the most severe effects on array radiation patterns were due to inaccuracies in element phases. The sidelobe level, that turned out to be the most sensitive parameter, increased several decibels when the maximum phase errors were more than 10 degrees. Beam mispointing and reduced directivity seem to be of minor concern. Even maximum phase errors of 45° do not turn the main beam more than 1°. Amplitude errors and errors in element positions had very little effect on the radiation characteristics.

4 Array measurement system

In this work an antenna array testbed for antenna design and testing, and radio channel modeling purposes is investigated. The testbed is based on the wideband radio channel sounder developed at Institute of Radio Communications (IRC), Helsinki University of Technology (HUT). An extension of the system for array measurements is implemented in this work. During the channel measurements the transmitter of the sounder is moved around, and the array simulating a BS antenna is connected to the receiver. The angular distribution of the received signal components can be solved by comparing the relative phases of the element signals. Furthermore, the wideband sounding also provides the delay information, and thus a two-dimensional characterization of the propagation channel is possible. The testbed also provides the possibility to study the effects of different array geometries on the operation of adaptive arrays. The purpose of the work is to identify the advantages and limitations of the system.

4.1 WIDEBAND RADIO CHANNEL SOUNDER

The complex impulse response (IR) of the radio channel can be computed as a cross-correlation of the transmitted and received signals. The impulse response contains a lot of valuable information of the channel: delay spread, Doppler spread, etc. The channel sounder consists of one transmitter and one receiver accompanied by a control computer [53,54]. The carrier frequency is 2.154 GHz with 100 MHz bandwidth (upper UMTS band). Maximum transmission power is limited to 10 W. A simplified block diagram of the system is given in Figure 4.1.

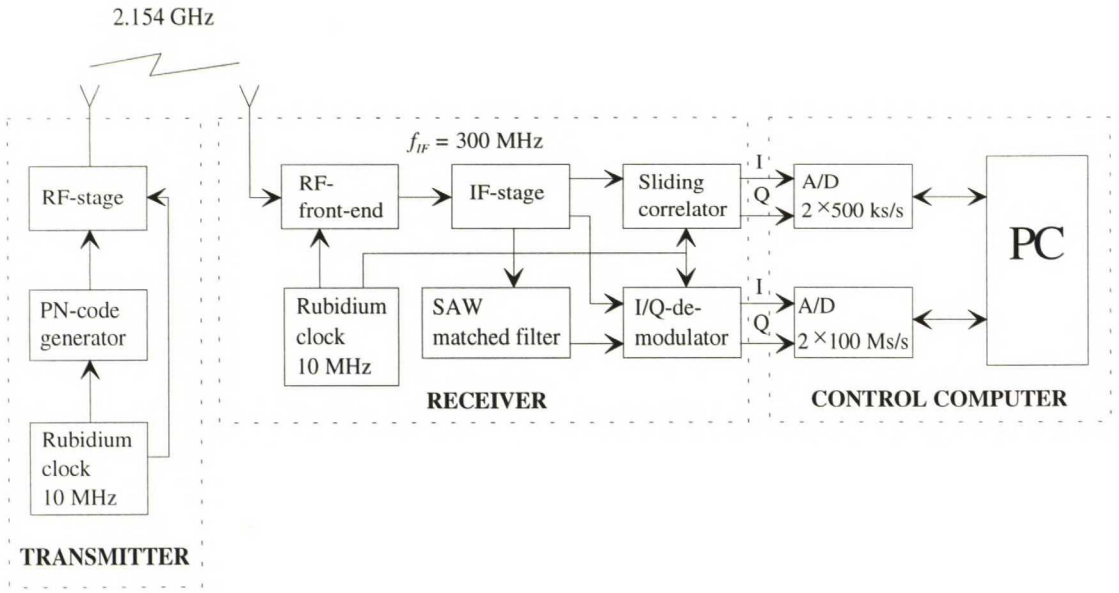

Figure 4.1. *Simplified block diagram of the channel sounder [55].*

In the transmitter the carrier frequency is modulated with a periodically repeated pseudo noise (PN) -code. In the receiver the downconverted signal is either correlated with a locally generated replica of the PN-code, or it is sampled directly and the correlation is calculated with post processing. Depending on the current setup, either the sampled IRs, or the samples of the signal are stored to the hard disk of a PC. The receiver is equipped with Automatic Gain Control (AGC) to keep the signal level inside the input range of the ADCs. The AGC values are stored together with the IR/signal samples.

The transmitter and receiver are synchronized by separate 10 MHz rubidium standards to preserve the phase information. The reported Allan variance of the clock frequency is $3 \cdot 10^{-11} / \sqrt{t}$, for $1\text{s} \le t \le 100\text{s}$. The stability is $2 \cdot 10^{-11}$ / day and $2 \cdot 10^{-9}$ / year. The temperature drift is $\pm 3 \cdot 10^{-10}$ Hz in the range of -5°C...+50°C. Before every measurement, the clocks have to be tuned to minimize the difference in the frequencies in the transmitter and the receiver. According to [55] the practically achievable frequency offset is about 30 mHz. In short-range indoor measurements (e.g. in an anechoic chamber) the tuning is not necessary, because the transmitter and receiver can be synchronized by using a cable to connect the transmitter clock also to the receiver.

4.1.1 Sliding correlator receiver

In this work the measurements were performed with the sliding correlator receiver [53,55]. In the sliding correlator the 300 MHz IF-signal is correlated with another 300 MHz IF-signal up-converted from a local PN-code generator. The output of the sliding correlator is sampled using two 12-bit ADCs with a maximum sample rate f_s = 500 kHz before storing to hard disk. The chip frequency of the PN-code is f_c = 53.85 MHz, and the length of the code sequence is L_c = 1023 bits. The nominal delay resolution is $\tau_{\min} = 1/f_c$ = 18.6 ns. The delay range, i.e. the maximum value of an unambiguous delay is 19.0 µs, which is in practice a lot longer than required. In the measurements a time window of 1.9 µs was used to limit the amount of the data. The nominal measurement rate f_m for the sliding correlator receiver is written as

$$f_m = \frac{f_c}{KL_c} \tag{4.1}$$

where K is a scaling factor, that compresses the bandwidth of the output waveform of the sliding correlator. The value of the scaling factor used in the measurements was K = 1077. With the values above the theoretical measurement rate is 48.9 Hz. In practice, the maximum achievable frequency is 24 Hz, when only 10 % of the code is sampled with a sampling frequency of 200 kHz. The resulting delay range is 2 µs. The reason is the limited speed in transferring data to the hard disk. Respectively, if a 4 µs delay range is desired, the measurement rate becomes 12 Hz. Due to the principle of operation of the sliding correlator, it produces self noise. The level of the self noise is approximately 23 dB below the peak of the main signal component [56], and it has to be cut out from the results.

4.1.2 Direct sampling receiver

If the receiver is used in the direct sampling (DS) mode, no PN-code generation is required in the receiver. Instead, the IF is I/Q-demodulated and the I- and Q-channels are sampled directly using two 8-bit ADCs with a maximum sample rate f_s = 100 MHz. The IRs are calculated with post processing. Because the codes in the transmitter and receiver are no synchronized, at least 3 successive IRs have to be recorded from each ele-

ment. This also compensates the differing propagation delays. Because of the very high-rate sampling, the samples of the signals are not directly transferred to hard disk, but stored in fast memory buffers. Currently the size of the memory buffer is 2 Mbytes for both channels. With the highest possible sampling rate this leads to only 20 ms continuous measurement time. After this the measurement has to be paused while the data is transferred to hard disk. In DS-mode the code length and the chip frequency can be chosen more freely, thus allowing the optimization of the measurement rate with respect to the maximum Doppler frequency, or required delay resolution (see Sec. 4.2.2). This is essential because of the limited data storage capability. The nominal measurement rate of the DS receiver is

$$f_m = \frac{f_c}{L_c} \tag{4.2}$$

The maximum measurement rate is achieved with f_c = 60 MHz and L_c = 31 bits, and is 1.94 MHz. The minimum delay resolution is 16.7 ns corresponding to the highest chip frequency. The delay range is the inverse of the measurement rate.

In addition to direct sampling, matched surface acoustic wave (SAW) filters can be used before the I/Q demodulation. The two existing filters are matched to two codes: a 13-chip 2.5 MHz Barker code and a 127-chip 10 MHz m-sequence. In this case the demodulated signals give the complex IRs.

The available options for measurement parameters with the sliding correlator receiver and the direct sampling receiver are summarized in Table 4.1.

Table 4.1. *Available options for measurement parameters.*

	Sliding correlator	Direct sampling
Code length	1023	31-2047
Chip frequency [MHz]	53.85	2.5-60
Delay range [μs]	19	0.5-819
Delay resolution [ns]	18.6	16.7-400
Maximum sampling rate [MHz]	0.5	100
Maximum measurement rate [Hz]	49	$1.94 \cdot 10^6$
Dynamic range [dB]	30	30

4.1.3 Sounder extension for array measurements

In order to measure multiple antenna elements with a single receiver, a fast RF switching unit is required behind the antenna. The used switching unit [57] is based on a TTL-controlled GaAs switch (Mini-Circuits VSW 2-50 DR) has 8 channels and a switching time of 3 ns. The input ports of the switching unit are matched to 50 Ω. The return loss is more than 10 dB over the whole frequency band of the transmitted signal, no matter whether the channel is selected or not. The matching is important if mutual coupling effects in an array are to be measured. The minimum isolation between the channels of the switching unit is as poor as 20 dB, and is mainly caused by the used switching component. The isolation limits the capability of the system to measure mutual coupling effects. A better switch will be designed in the future, and the system will be extended for measuring larger arrays.

The switching unit is controlled by a 3-bit TTL-signal. The control signal is generated from a pulse-per-sequence (PPS) -signal triggered by the sampling card of the receiver. The number of subsequent IRs measured from each element before switching to the next can be selected in the range of 2...16. In addition to the PPS, another signal is required for correct timing when the measurement is started. This RESET-signal is triggered by the PPS.

In array measurements the concept of measurement rate becomes ambiguous. To clarify the terminology, Table 4.2. describes some terms and corresponding symbols that are frequently used in the following sections.

Table 4.2. *Terminology related to measurement rates in array measurements.*

Symbol	Description of meaning
f_m	The nominal measurement rate, i.e. the inverse of the time between two measured consecutive impulse responses.
$f_{m,e}$	Achieved practical rate of measuring IRs from successive elements. Equals to the maximum switching frequency of the array.
$f_{m,a}$	Achieved practical rate of measuring IRs from each element of the whole array.

4.2 PERFORMANCE CONSIDERATIONS

To evaluate the performance of the testbed its inherent error sources have to be identified. The sensitivity of radiation patterns of uniformly illuminated arrays to random phase and amplitude errors in element signals are investigated in [21] (see Sec. 3.5.3). The main conclusions were that phase errors are the most severe ones and the most sensitive characteristics are the sidelobe level and the directivity. The effect is stronger for smaller number of elements. Random rms amplitude variations up to 3 dB had almost no effect on the radiation pattern. Respectively, random rms phase errors smaller than 10° turned out to have small effect. The rise in the sidelobe level was less than 1 dB. These values are considered as references when evaluating the performance of the testbed. It must be noticed, however, that the error tolerances become smaller if optimized patterns with e.g. lower sidelobe levels are desired.

If the phase errors are not random, but all of the same size and to the same direction, the result is a shifted beam pointing angle. Errors of this kind are here called cumulative phase errors. In this case the relative error is stronger for larger arrays because of the narrower beam. The relative beam mispointing can be written as a function of the cumulative phase error $\Delta\phi$ by

$$\frac{\Delta}{HPBW} = \frac{L}{0.886 \cdot d} \cdot \frac{\Delta\phi}{360°} \tag{4.3}$$

for

$$\Delta\phi << \frac{d}{\lambda} \cdot 360°$$

If the desired maximum beam mispointing is 10 % of the 3 dB beamwidth, the maximum cumulative phase error becomes

$$\Delta\phi_{max} = \frac{d}{L} \cdot 31.9° = \frac{31.9°}{N-1} \tag{4.4}$$

which gives 4.6° for an 8-element array.

4.2.1 Phase accuracy of clocks

The frequency offset between the clocks in transmitter and receiver can be tuned down to 30 mHz. The resulting phase rotation (~11°/s) is quite linear and can thus be removed, if necessary, by comparing two subsequent IRs from one element. Assuming that the array has 8 elements and no correction is done, the maximum measurement rate $f_{m,e}$ must be as slow as 2.4 Hz in order to achieve 10 % accuracy in beam pointing direction.

Also the phase noise of the clocks in transmitter and receiver limits the accuracy of the measured phase. The measured rms phase error for different configurations is presented in Table 4.3. In the measurement, 5000 IRs were recorded with the sliding correlator receiver. The measurement rate was 24 IRs/s. The transmitter and receiver were connected together with a cable. The slow phase variation due to the frequency offset has been filtered out.

Table 4.3. *Measured root-mean-square phase error of the sounder.*

	$\Delta\phi_{rms}$
subsequent IRs	1.39°
every 8th IR	2.16°
3 averaged IRs from subsequent elements	1.45°
3 successive IRs averaged from every 8th element	1.65°

Table 4.3 indicates that the rms phase error increases with increasing time between measurements. Averaging improves the performance if the time between the measured IRs is long enough. Instead, if closely measured IRs are averaged, the increased time between IRs outweighs the gain due to averaging.

The measured frequency spectrum of the oscillator of the receiver [58] is shown in Fig. 4.2.

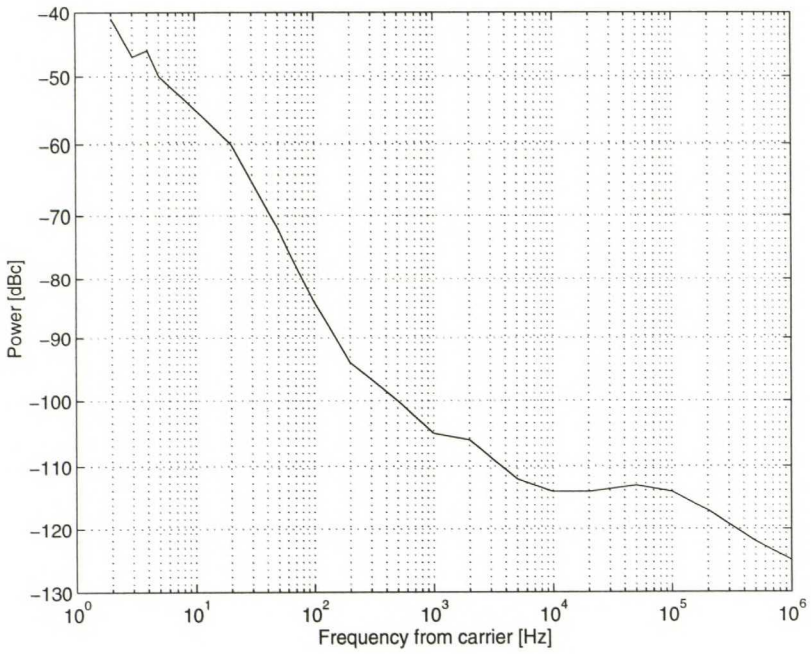

Figure 4.2. *Phase noise of oscillator of receiver.*

The noise variance can be written approximately as [59]

$$\sigma_n^{\,2} = \sum_i \left\{ \begin{array}{l} 10^{\frac{\mathrm{dBc}_i}{10}} f_i \log\frac{f_{i+1}}{f_i} \rightarrow x = -1 \\ 10^{\frac{\mathrm{dBc}_i}{10}} \frac{f_i}{x+1}\left[\left[\frac{f_{i+1}}{f_i}\right]^{x+1} - 1\right] \rightarrow x \neq -1 \end{array} \right\} \tag{4.5}$$

where

$$x = \frac{\mathrm{dBc}_{i+1} - \mathrm{dBc}_i}{10\left(\log f_{i+1} - \log f_i\right)}$$

The rms uncertainty is the same as the standard deviation σ_n. Equation (4.5) gives a single sideband (SSB) value that has to be multiplied by $\sqrt{2}$ to get the DSB value. Assuming that the uncertainties in transmitter and receiver are independent, the total phase error in the measurement is obtained by multiplying again by $\sqrt{2}$. Thus, the rms value of the phase uncertainty becomes

$$\Delta\phi_{\text{rms}} = 2 \cdot \sigma_n \tag{4.6}$$

Calculating the noise variance σ_n^2 from the measured frequency spectrum gives $\Delta\phi_{\text{rms}} =$ 1.34°. This is slightly smaller than that in Table 4.3 for two subsequent measurements. The difference may be caused by the noise added e.g. in the sliding correlator. Altogether, the values are negligible when considering radiation pattern distortions.

4.2.2 Effect of feed network

In the existing configuration the array elements are connected to the switching unit by semi-rigid coaxial cables. The cables are not equally long, which changes the relative phases of the element signals. Therefore, the phase increments added by the cables have to be removed from the results to get the phases correct. The small transmission loss of the cables is fixed over the frequency band. It can thus be corrected simply by adding the loss to the measured IRs.

Also the different channels of the switching unit have different transmission characteristics that affect the recorded signals. Figure 4.3 presents the frequency responses of the transmission loss of different channels measured with a network analyzer.

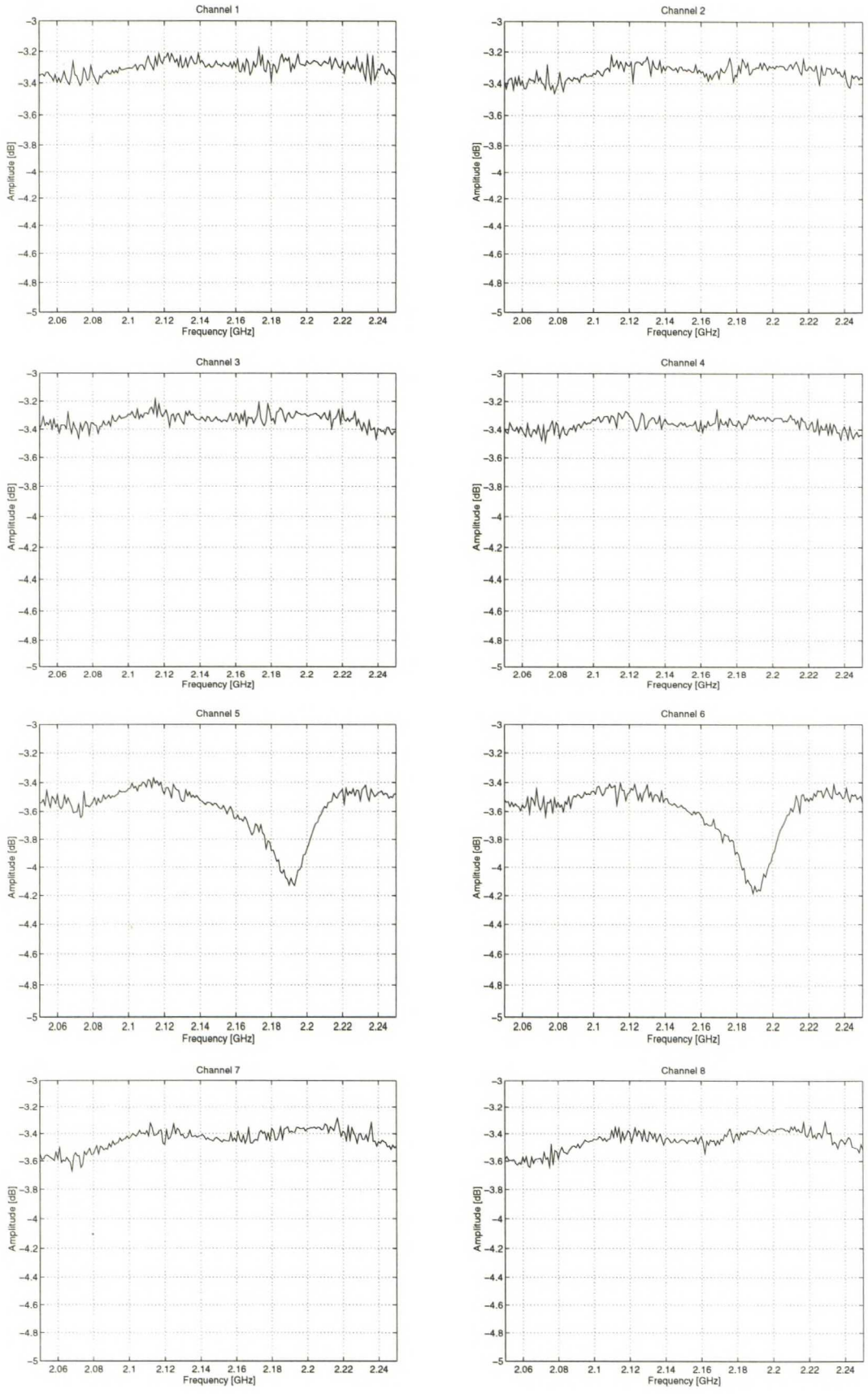

Figure 4.3. *Frequency responses of transmission loss of different channels in switching unit.*

As can be seen the frequency responses are not identical. For example, channels 5 and 6 have a 0.7 dB resonance dip at 2.19 GHz. It can be compensated by correcting the results with the measured transmission properties. Because of the wideband signal, the correction should be done over the whole frequency band to get results that are exactly correct. This can be done using Fourier transform

$$r(\tau) = \mathcal{F}^{-1}\left\{\frac{\mathcal{F}\{r_m(\tau)\}}{H_{feed}(f)}\right\}, \qquad (f_0 - f_c) \le f \le (f_0 + f_c) \tag{4.7}$$

where $r_m(\tau)$ is the measured impulse response and $H_{feed}(f)$ is transmission function of the feed network containing both the switching unit and the feed cables. $\mathcal{F}$ and $\mathcal{F}^{-1}$ represent Fourier transform and inverse Fourier transform, respectively.

In the practical measurement examples of this work the results are corrected only at the carrier frequency f_0 (2.154 GHz) for simplicity. To test the effect of the different channel characteristics, a measurement was performed in an anechoic chamber with the transmitter antenna at broadside direction. Figure 4.4 shows the average of 40 measured impulse responses from channels 1 and 5 without correction. Figure 4.5 shows the same IRs corrected at the center frequency.

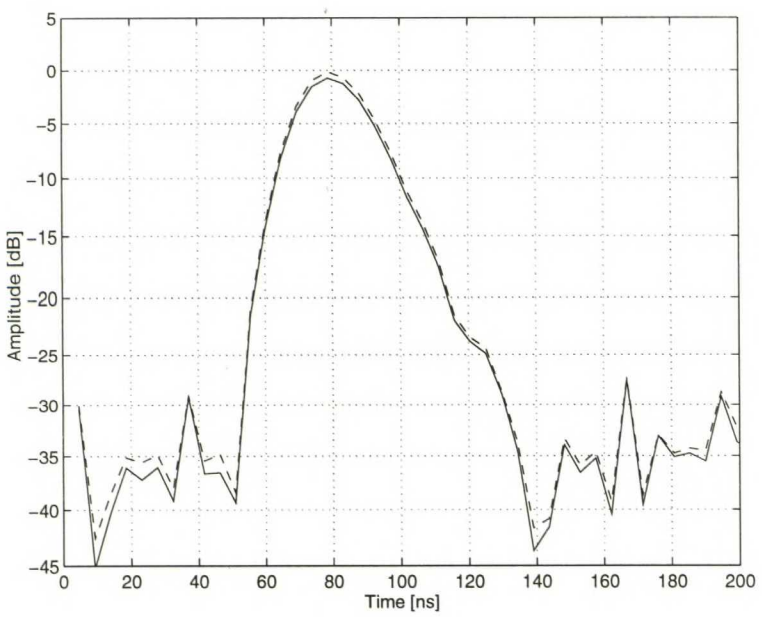

Figure 4.4. *Measured IRs. Solid line represents channel 1, dashed line channel 5.*

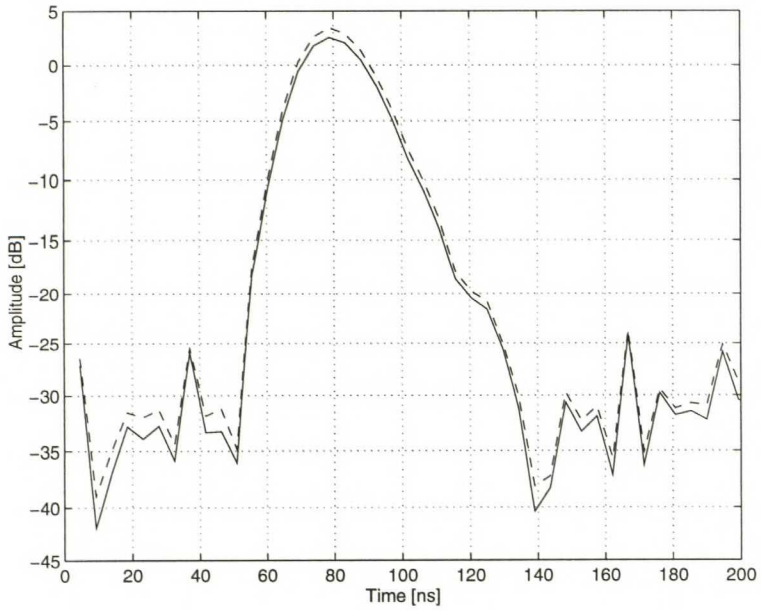

Figure 4.5. *IRs corrected at center frequency. Solid line represents channel 1, dashed line channel 5.*

Without correction the peak level of the signal received from channel 5 is about 0.7 dB higher than that from channel 1. This can not be caused by the switching unit, because channel 1 has smaller transmission loss at center frequency (see Fig. 4.3). Consequently, the difference is even larger after the correction, approximately 1 dB. The reason for the difference in signal levels is so far unknown. It may be caused by mismatches between the components, or overcoupling either in the array or in the switching unit. The reason will be further investigated in the future. As mentioned in the beginning of this section, amplitude errors of this order (±1 dB) should not affect the measured angular distributions of received signals. However, the error tolerances are smaller for optimized radiation patterns. The shapes of the impulse responses are very similar. This indicates that the frequency dependent transmission loss of channel 5 has little effect on the results.

4.2.3 Effect of Doppler spectrum

The impulse responses of the radio channel are not measured exactly at the same time from each element of the array. This means that some assumptions of the rate of change of the channel have to be made. In practice, the type of the environment and the speed of the mobile determine the width of the Doppler spectrum. If LOS exists and reflections

can be neglected, the Doppler spectrum consists of only one single spectral line. This Doppler shift can be resolved by comparing the phase difference between IRs from subsequent sweeps in one element of the array. Because of the single frequency component, the phase rotation is linear between the ends of the array. One can thus remove the Doppler phase rotation from the element signals to solve the DOAs. In such case, the required array measurement rate $f_{m,a}$ is twice the maximum Doppler frequency. In more practical case the signal experiences multiple reflections from moving objects which causes spreading of the Doppler spectrum. In this case, the phase rotation is not linear and can not be separated from the phase difference that depends on the DOA of the signal. Figure 4.6 shows the misalignment of the measured impulse responses in the time domain.

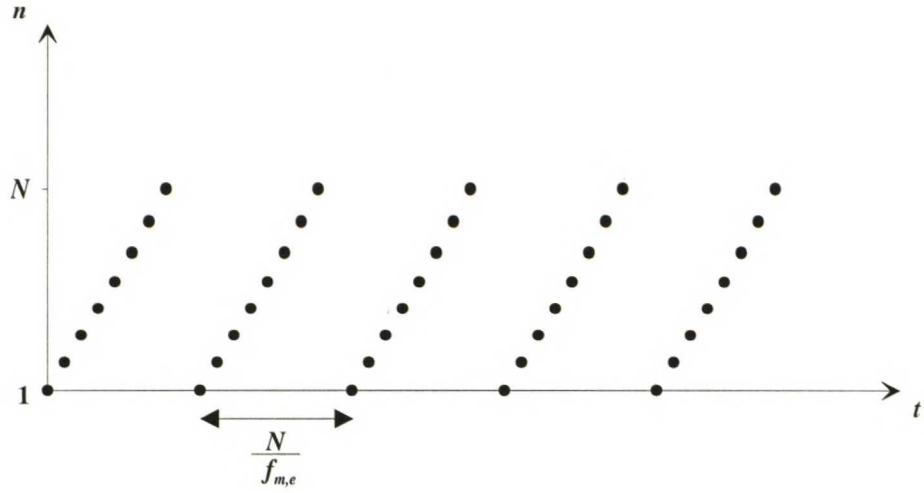

Figure 4.6. *Misalignment of IRs in time domain.*

The accuracy of the measured phases of the signals depends on the measurement rate. The maximum possible phase shift between the first and last element of the array is

$$\Delta\phi_{\text{tot,max}} = \frac{f_{D,\max}}{f_{m,a}} \cdot 360° \tag{4.8}$$

where $f_{m,a}$ is array measurement rate and $f_{D,\max}$ is maximum Doppler frequency written as

$$f_{D,\max} = (N_R + 1) \cdot \frac{v_{\max}}{\lambda} = (N_R + 1) \cdot f_0 \cdot \frac{v_{\max}}{c} \tag{4.9}$$

where v_{max} is the maximum speed of the mobile, f_0 is carrier frequency, and c is speed of light. Coefficient N_R is the number of reflections from other objects moving at the same speed as the mobile. In practice, the maximum value of N_R is 1...2, while the most common value is $N_R = 0$.

The maximum phase shift between two array elements becomes

$$\Delta\phi_{max} = \frac{f_{D,max}}{f_{m,a}} \cdot \frac{360°}{N} \tag{4.10}$$

To get the element measurement rate $f_{m,e}$, the array measurement rate has to be multiplied by the number of elements. Thus, the required element measurement frequency to achieve desired accuracy becomes

$$f_{m,e} = (N_R + 1) \cdot f_0 \cdot \frac{v_{max}}{c} \cdot \frac{360°}{\Delta\phi_{max}} \tag{4.11}$$

The phase error leads to inaccurate DOA information. The maximum cumulative phase error for a given beam pointing accuracy can be calculated using Eq. (4.4). For an 8-element array, to achieve a maximum of 10 % beam pointing error, the maximum cumulative phase error becomes $\Delta\phi_{max} = 4.6°$. The requirement is alleviated for random errors.

With the sliding correlator receiver, the maximum practical measurement rate $f_{m,e}$ is about 24 Hz. According to Eq. (4.11), the maximum mobile speed is 0.017 m/s, assuming that $N_R = 1.5$ and $\Delta\phi_{max} = 4.6°$. In practice, only static array measurements are possible with the sliding correlator. Instead, the direct sampling receiver allows fast channel sounding with the cost of a short continuous measurement time. Table 4.4 presents the maximum mobile speed v_{max}, delay range τ_{max}, and the resulting continuous measurement time t_m for a given system configuration, when 3 successive IRs are recorded from each element. The maximum allowed beam mispointing error is 10 % of the *HPBW*, the array has 16 elements, and $N_R = 1.5$.

Table 4.4. *Delay resolution, delay range, maximum mobile speed, and continuous measurement time for different configurations of the DS receiver.*

f_c [MHz]	L_c [bits]	f_s [MHz]	τ_{min} [ns]	τ_{max} [μs]	v_{max} [m/s]	t_m [ms]
2.5 MHz	31 - 255	5 MHz	400	12.4-102	8.85 - 1.08	400
10 MHz	31 - 1023	20 MHz	100	3.10-102	35.4 - 1.07	100
30 MHz	31 - 2047	60 MHz	33.3	1.03-68.2	106 - 1.61	33
60 MHz	31 - 2047	100 MHz	16.7	0.52-34.1	212 - 3.22	20

As shown in Table 4.4, the maximum mobile speeds can be very high. The corresponding delay ranges are, however, infeasibly short. Also, the continuous measurement times are very short because of the limited memory buffer. Therefore, the IRs are recorded in sets. This means that after measuring 3 IRs from every element, there is a short break before recording the next set. By this way, the measurement time can be increased. Of course the maximum mobile speed decreases at the same time. The desired measurement characteristics have to be determined very carefully for every measurement setup to maximize the measurement time and minimize the amount of data.

4.3 Advantages of multi-element sounding

The possibility to measure complex impulse responses separately from each element of an array provides insight in multipath radio channels and serves as a tool for developing adaptive BS antennas. The measurement data is available for post processing and can be used for various purposes. Radio engineers obtain real information of the functionality of their hardware, DSP engineers can test adaptive algorithms, and system designers increase their knowledge about radiowave propagation in difficult environments.

4.3.1 Antenna development

The main purpose of an adaptive base station antenna is to produce a large number of narrow beams with as few elements as possible. If digital beamforming is considered, the number of required tranceivers is the same as the number of array elements. Therefore, it is important to find array geometries that do not waste elements. The testbed allows the possibility to study different geometries and element numbers. Also the effects of mutual coupling can be investigated. For example, blind angles can be found by ro-

tating the receiving array in front of a known source. Furthermore, the benefits of the polarization adaptivity / diversity as well as the usefulness of thinned receiving arrays can be analyzed. In addition to BS antenna measurements, also adaptive mobile antennas can be studied in the future.

4.3.2 Adaptive antenna simulations

An adaptive antenna is mainly a signal processing system. It requires a great deal of computational power and efficient signal processing algorithms to be implemented efficiently. With the multi-element measurement system, the functionality of adaptive beamforming algorithms can be tested in practice, because the data produced by the sounder is real radio channel data. To simulate a multi-user situation one can record short sequences of data at different mobile locations and then combine all sequences. One signal source is treated as the desired user, and the others as interferers. The real *SINR* can be calculated for each user before and after the beamforming. In addition to one BS, also whole networks employing adaptive BS antennas can be simulated.

4.3.3 Channel modeling

The multi-element sounding allows the possibility to study the signal propagation characteristics in different environments. For example, the angular spreading of the signal can be measured. The results can be used to determine the minimum practical beamwidth of the array in various environments. Because the data is post processed numerically, the same freedom in radiation pattern synthesis is available as with DBF. For example low-sidelobe patterns can be produced separately for each user. The main limitation is the size of the antenna used in the measurements (unless superresolution is considered).

Due to the wideband sounding (BW = 100 MHz), the correlation between signals in different frequencies can be studied. By filtering the sampled signal with two narrow-band filters with center frequencies separated e.g. 50 MHz, the fading characteristics of the signals at different frequencies can be studied separately. This can be used to find out the correlation properties of the up- and downlink signals in FDD systems.

5 Measurements

5.1 PROTOTYPE ARRAY

A prototype array has been designed and built for first measurements and testbed evaluation. The array has 16 elements in two horizontal rows. The element spacing in both rows is $\lambda/2$ but the rows are horizontally shifted by $\lambda/4$ relative to each other. This allows more options for selecting the element spacing. The vertical spacing between the rows is about $\lambda/2$, which is assumed to be small enough to get correlated signals. The polarization is vertical and the array will thus be scanned in H-plane.

The element used is a probe-fed short-circuited quarter-wave microstrip patch with air substrate. It was selected because it is fairly easy to manufacture and has moderately wide bandwidth. The dimensions of the element are: height 10 mm, width 25 mm, and length 33 mm. The array is made of 0.5 mm thick copper plate, to the edges of which the elements are shorted. The size of the array is 150 mm $\times$ 645 mm. The elements are fed with SMA coaxial connectors from behind the ground plane, and connected to the switching unit by semi-rigid coaxial cables. The array and the switch are both mounted on an aluminum support. Figures 5.1 and 5.2 present the configuration.

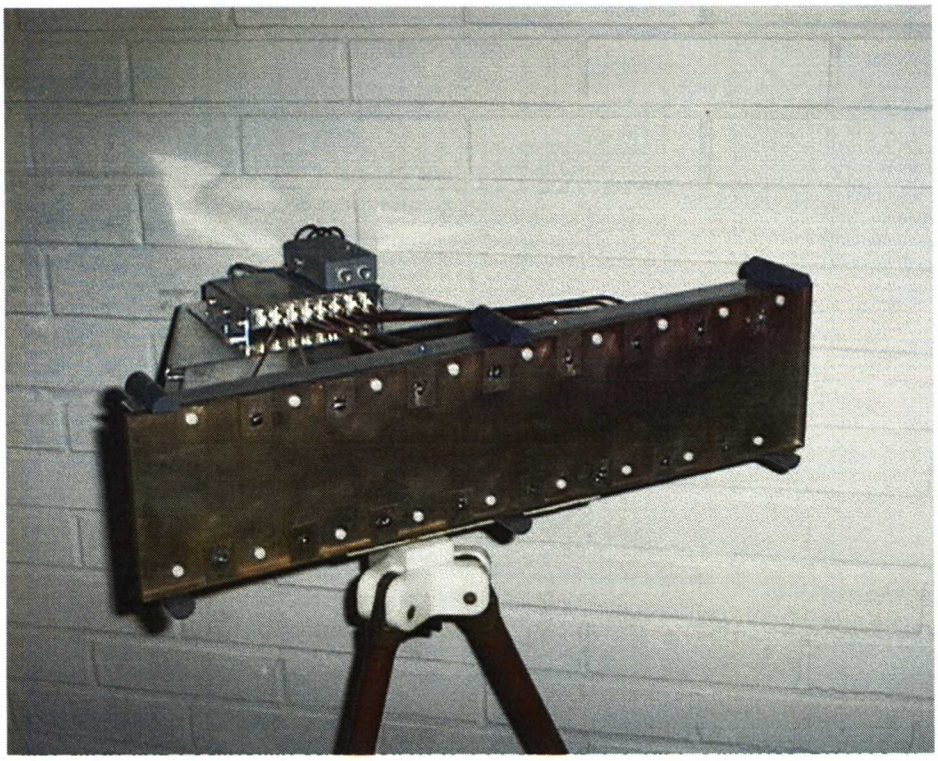

Figure 5.1. *Prototype array used in the measurements.*

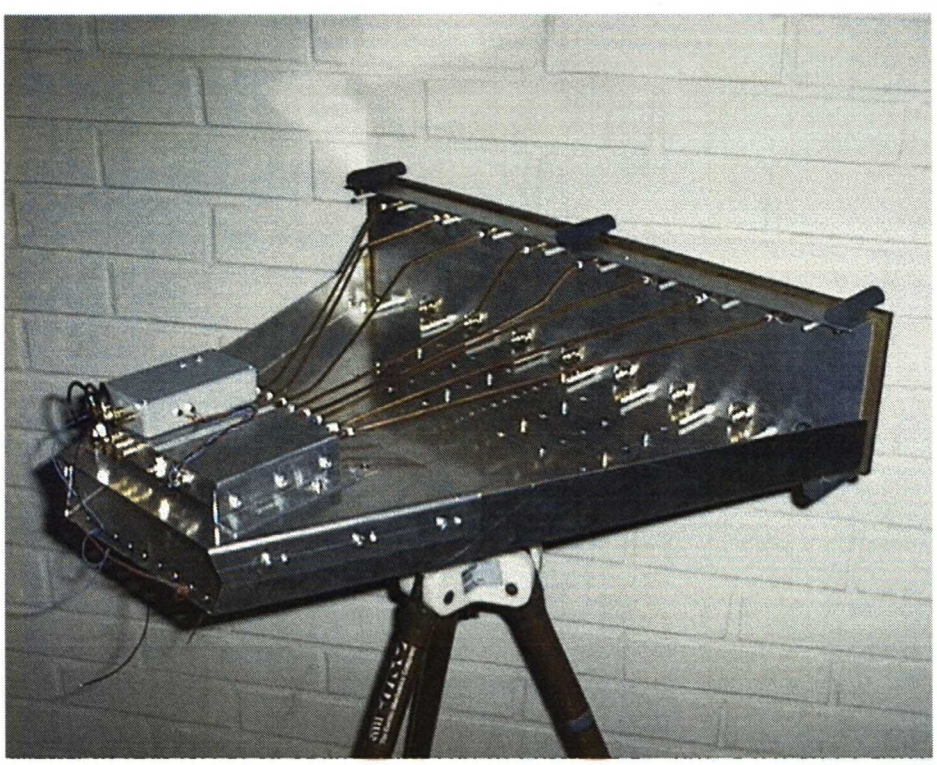

Figure 5.2. *Array feed network and switching unit.*

The resonant frequency of the elements was tuned by adjusting the length of the patches. The input impedance was matched by changing the distance of the connection point of the coaxial probe from the short circuit. Figure 5.3 shows the input reflection coefficients measured with a network analyzer from 4 different elements in the array.

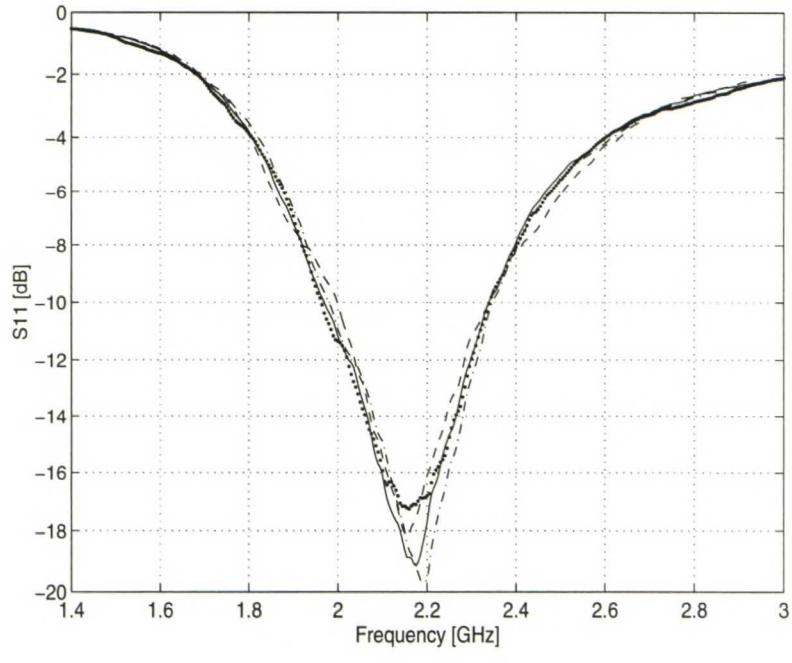

Figure 5.3. *Measured input reflection coefficient of different elements.*

As shown in Fig. 5.3 the return loss is more than 15 dB over the 100 MHz measurement bandwidth (2154 ± 50 MHz). The radiation patterns of some of the array elements were measured in the anechoic chamber at HUT Radio Laboratory. The H-plane radiation pattern of both a center element and an edge element at 2.154 GHz frequency are shown in Figures 5.4 and 5.5. The edge element has wider beam than the center element. This is caused by the coupling from surrounding elements. The 3 dB beamwidth of the edge element is about 91°, while in the center element it is only 83°.

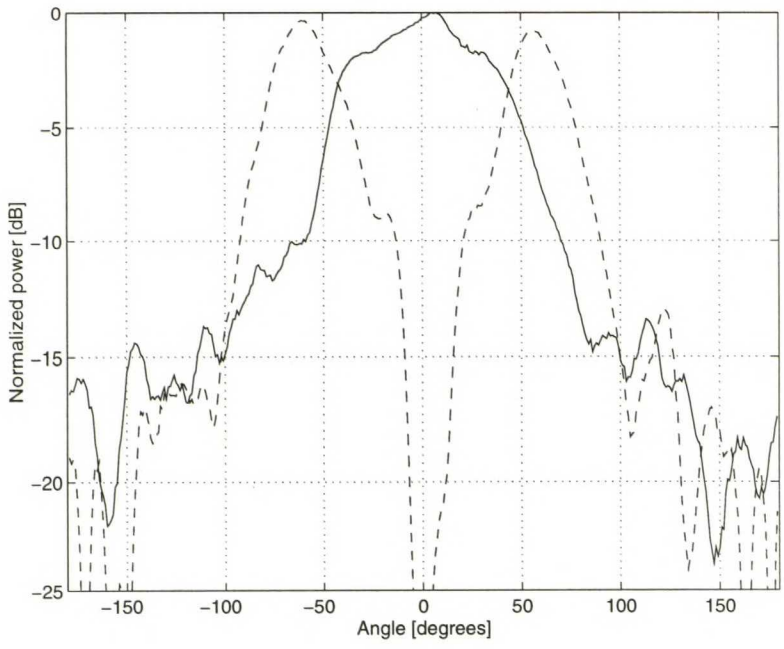

Figure 5.4. *Radiation pattern of center element of the array at 2.154 GHz. Solid line represents the main polarization, dashed line the cross polarization*

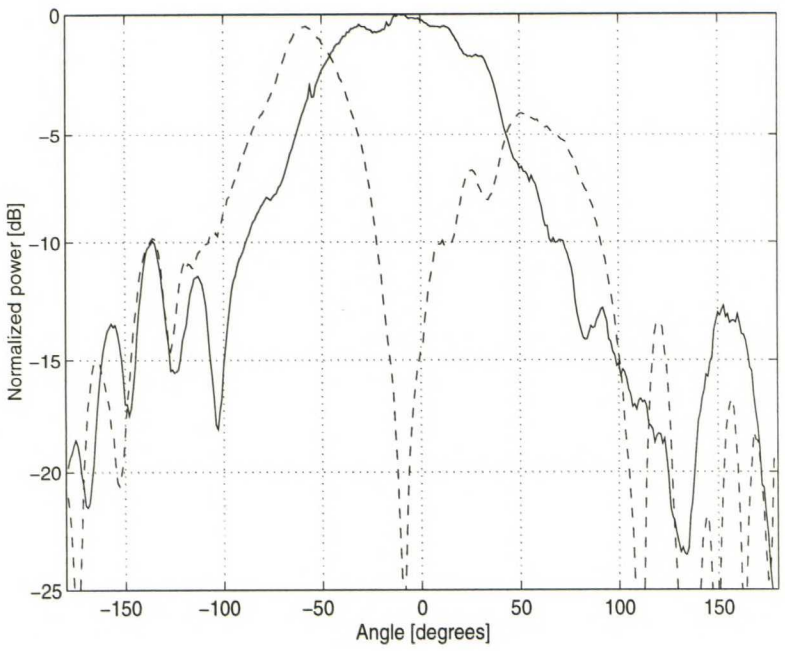

Figure 5.5. *Radiation pattern of edge element of the array at 2.154 GHz. Solid line represents the main polarization, dashed line the cross polarization*

As can be observed the cross polarization is considerably higher at certain directions than the main polarization. This is assumed to be caused by the relatively high element and the coaxial feed probe of the element that behaves as a horizontal monopole. The monopole has a pattern null in the direction of its axis, which explains the shape of the cross polarization pattern. Because of the poor polarization characteristics, the data measured with the prototype array does not correspond completely to the real situation. Although the prototype can be used for testing of the measurement system, a better array will be developed in the future.

5.2 MEASUREMENT SETUP

During the testbed measurements only the elements at the upper edge of the array were connected to the switch. In other words, the antenna was used as an 8-element linear array with $\lambda/2$ element spacing. The elements in the other row were terminated with matched 50 Ω loads. The measurements were performed with the sliding correlator receiver. The parameters used are presented in Table 5.1.

Table 5.1. *Parameters used in the measurements.*

Code length	1023
Scaling factor	1077
Delay resolution	18.6 ns
Delay range	1.9 μs
Array measurement rate	1.5 Hz

The array measurement rate in Table 5.1 results from an element measurement rate of 24 Hz, when recording two successive IRs from every element before switching to the next. In practice, only static measurements are possible with this configuration.

5.3 ARRAY PATTERN MEASUREMENT

The first measurements were performed in the anechoic chamber to check the operationality of the system. The receiving array was turned a certain angle for every measurement with respect to the transmitting monopole. A total number of 20 impulse responses were averaged at each angle point from all elements. The self noise of the receiver (see Fig. 4.4) was cut out from the results with a threshold of 25 dB below the peak of the main, and the IRs were averaged using Matlab. The transmission loss and phase shifts due to the feed network were compensated as described in the previous section. The result was one complex number from each element, i.e. the weight w_n (see Sec. 3.2.1). The corresponding array factor was synthesized by scanning the phase difference $\alpha = -kd\sin\theta$ (in Eq. (3.9)) over the corresponding angle $-90° \leq \theta \leq +90°$. The resulting array patterns are presented in Figure 5.6. Angle θ is presented on the horizontal axis. The transmitter was at direction θ_0 with respect to the receiver.

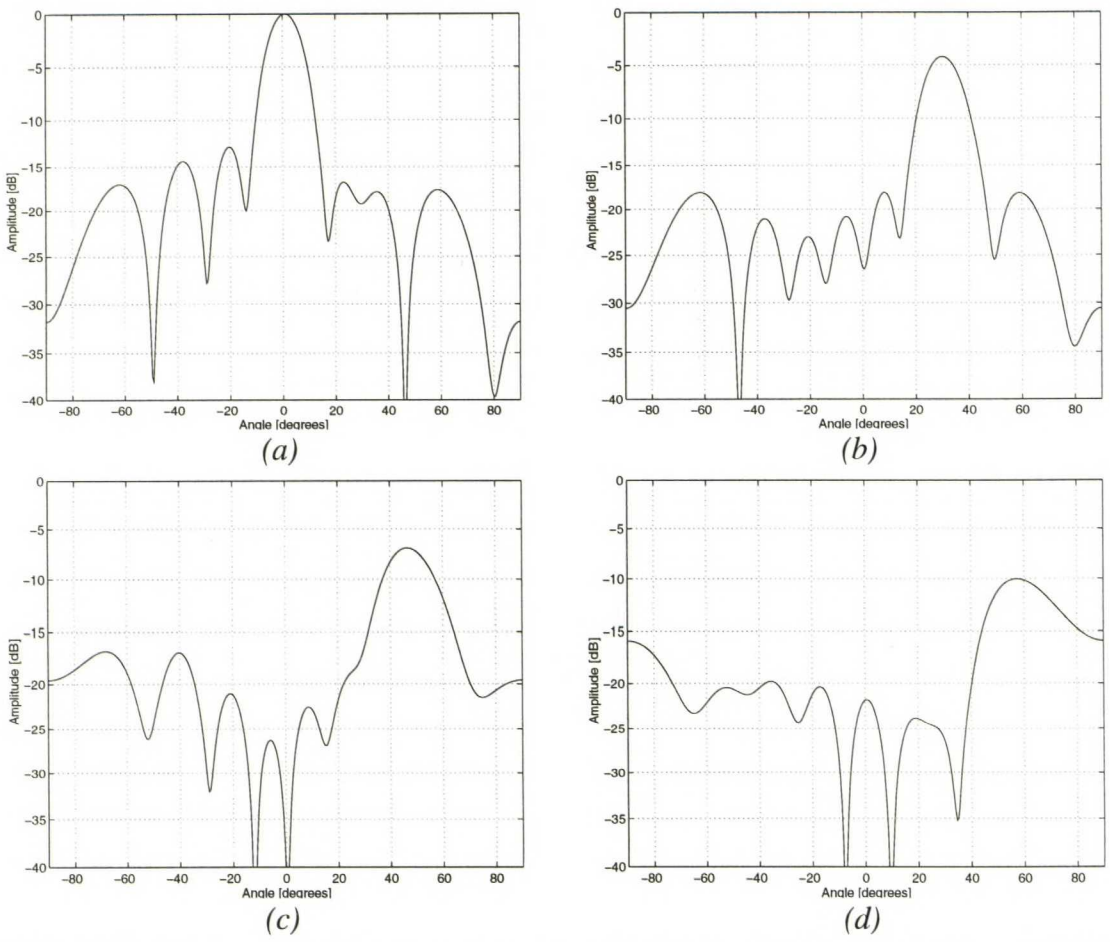

Figure 5.6. *Array patterns generated from measured element signals. (a) $\theta_0 = 0°$. (b) $\theta_0 = 30°$. (c) $\theta_0 = 45°$. (d) $\theta_0 = 60°$.*

The patterns are normalized to the maximum value of the pattern corresponding to $\theta_0 = 0°$ in Fig. 5.6. The drop in gain at wide scan angles (approximately 10 dB at 60°) matches fairly well with the measured element patterns in Figs. 5.4 and 5.5 (about -8 dB). The rest can be caused e.g. by scan-dependent impedance mismatches due to mutual coupling. The reason for the pattern distortion in the right sidelobes of Fig 5.6 (a) is not known. In Fig. 5.6 (b) the level of the first sidelobes is very close to the theoretical value (-13 dB below the main beam). Also the beamwidths match well the calculated ones. The 3 dB beamwidth of the array is about 13° at broadside and increases to 33° for $\theta_0 = 60°$. The theoretical values are 13° and 29°, respectively. The results indicate that the system is working as desired and the information is reliable up to scan angles of approximately ±60°, where the beam widening begins to limit the resolution.

The effects of amplitude and phase errors in the recorded signals were studied by weighting the signal amplitudes by Chebyshev coefficients to achieve low sidelobe patterns. The Chebyshev coefficients for both -25 dB and -30 dB sidelobes are presented in Table 5.2. The corresponding taper efficiencies are $\varepsilon_T = 0.896$ and $\varepsilon_T = 0.842$, respectively (see Eq. (3.30)).

Table 5.2. *Amplitude coefficients to obtain Chebyshev patterns.*

Element #	1	2	3	4	5	6	7	8
***SLL* = -25 dB**	0.370	0.572	0.825	0.980	0.980	0.825	0.572	0.370
***SLL* = -30 dB**	0.256	0.507	0.794	0.978	0.978	0.794	0.507	0.256

The resulting patterns for 20 averaged IRs from each element are shown in Figure 5.7.

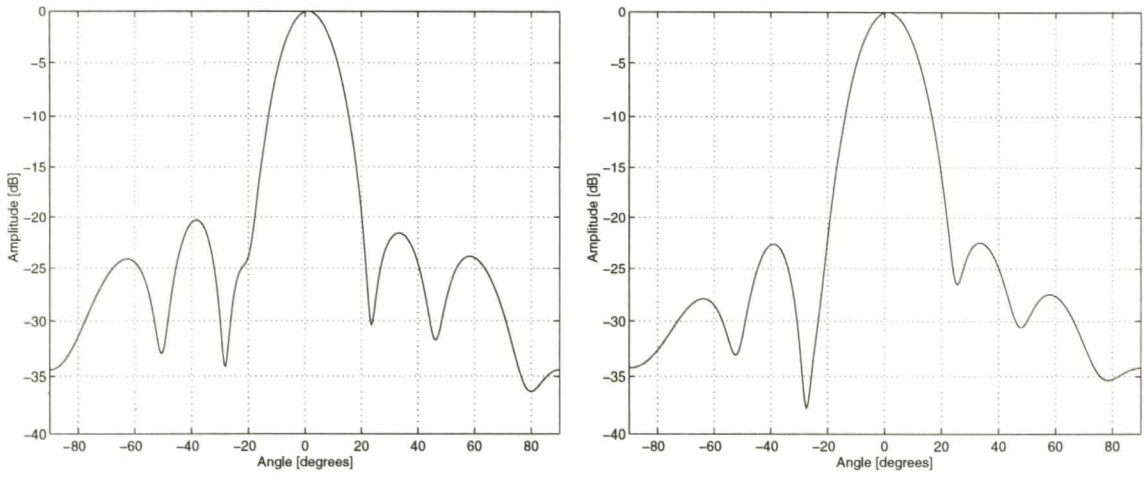

(a) *(b)*

Figure 5.7. *Chebyshev patterns synthesized from measured signals. (a) SLL =-25 dB. (b) SLL = -30 dB.*

It can be seen that the sidelobes are higher than desired. This is caused by errors in the received signals caused by the feed network. The levels of the highest sidelobes are about -20.3 dB and -22.4 dB. Solving Eq. (3.29) gives $\sigma = 0.054$ and $\sigma = 0.057$ for the rms error, respectively. This corresponds to 0.5 dB pure rms amplitude error, or 3.3° pure rms phase error. The amplitude and phase errors can not, however, be solved separately. The values are close to those obtained by test measurements in Chapter 4, although Eq. (3.29) is meant for large arrays.

5.4 EXAMPLES OF PRACTICAL MEASUREMENTS

After verifying that the system works it was tested in a more complex environment. The practical measurements were performed in the campus area of Helsinki University of Technology, in Otaniemi, Espoo, Finland. The receiving array was located on the roof of the main building of Department of Electrical and Communications Engineering, approximately 10 meters above ground level. The transmitter was positioned in various locations on ground level within the radius of a few hundred meters. The transmitter power level was 24 dBm. The environment type in the campus area is suburban. The buildings have a maximum of 3 stories, and their surroundings consists mainly of lawns and small forest areas. The impulse responses were recorded using the configurations

presented in Table 5.1. No Doppler compensation was used. Therefore, only two consequent IRs were averaged from each element during one sweep over the array.

The recorded element signals were weighted to obtain lower sidelobes. Chebyshev pattern with -25 dB nominal sidelobe level was used. This is a compromise between the narrower beam and lower sidelobes. Figure 5.8 shows the resulting array pattern of ideal array for two scan angles. The real broadside pattern looks more like that of Fig. 5.7 (a). The difference is in the sidelobe level, while the obtained beamwidth is close to the ideal one.

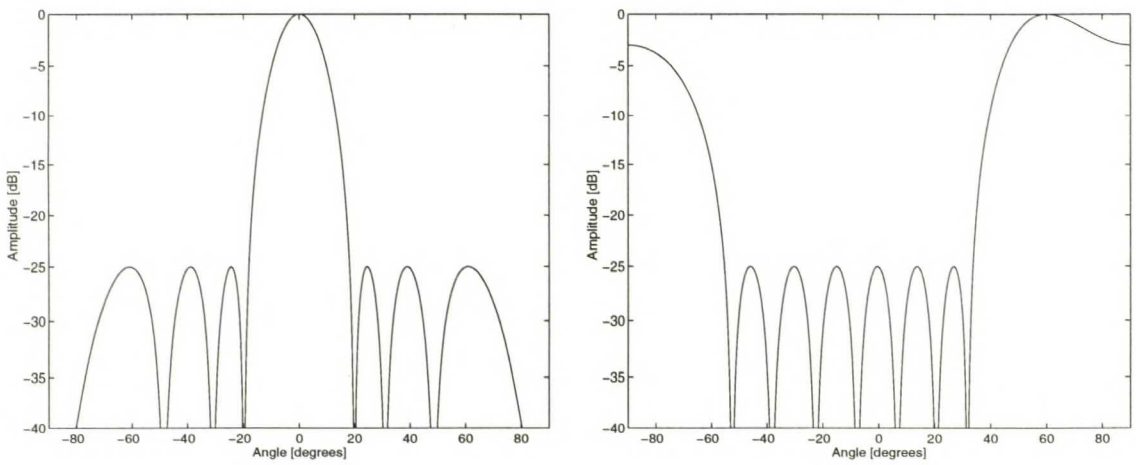

(a) *(b)*

Figure 5.8. *Ideal Chebyshev beam pattern. (a)* $\theta_0 = 0°$. *(b)* $\theta_0 = 60°$.

At broadside direction the resulting 3 dB beamwidth is about 15°. Instead, at 60° scan, the beam almost covers the whole sector up to 90°. Therefore, the signals received above ±60° are not reliable.

The location of the transmitter and a short description of the radio path from the transmitter to receiver are given in Table 5.3. The transmitter locations and the strongest signal propagation paths are shown in Appendix A.

Table 5.3. *Description of transmitter locations during measurements.*

Location #	Description of channel	Distance
1	LOS. 3-story building at left.	180 m
2	No LOS. Behind corner of a 2-story building.	190 m
3	No LOS. Several 3-story buildings between transmitter and receiver.	450 m
4	No LOS. High building at right.	70 m

The measured signals for various transmitter locations are shown in Figures 5.9 (a) - (d). The horizontal axis is the azimuth angle seen at the receiving array. The vertical axis is the time delay of the received signals. Because the system does not provide the absolute delays, the delays have been corrected to match the real situation. The maximum delay of 1900 ns corresponds to 570 meters. The measured signals presented are best understood when comparing to the physical situations in Appendix A. Transmitter locations 1-3 are shown in Figure A-1, location 4 in Fig. A-2. The position of the receiving array is the same for locations 1-3. The signals look like horizontal lines in Fig. 5.9 which limits the accuracy of resolving the directions. This is caused by the relatively wide beam of the 8-element array. Also the amplitude weighting widens the beam. Table 5.4 presents the approximate values of the peak directions of the measured signal components.

Table 5.4. *DOAs of peaks of received signal components.*

Location #	Straight component	Strongest multipath component
1	-21°	+27°
2	-4°	-6°
3	33°	(-34°)
4	+7°	-6°

In location 1, Fig. 5.9 (a), the reflection from the building at left from the transmitter is clearly seen (the component at +27°). The reflected signal is about 5 dB weaker than the straight component. The delay between the straight and reflected component is approximately 100 ns which corresponds to 30 meters. In addition, there is a weak back reflection component.

In location 2, Fig. 5.9. (b), the situation can be seen to be more complex. The delay spread is large and several signal paths exist. The possible propagation paths consist of e.g. the wall and roof-top diffraction from the building.

In location 3, Fig. 5.9 (c), the *SNR* is only 5 dB, and the noise level is notably higher than in the other locations. The weak component at -34° direction is received at almost the same time and seems to be an error.

In location 4, Fig 5.9 (d) the reflection from the wall at -6° is 10 dB stronger than the first component propagated through a roof-top diffraction or a straight path through the building.

As a conclusion it can be stated that the measured signals match very well the real situations and the testbed is working as desired. The developed system provides a novel approach to the two-dimensional analysis of the mobile radio channel in various environments.

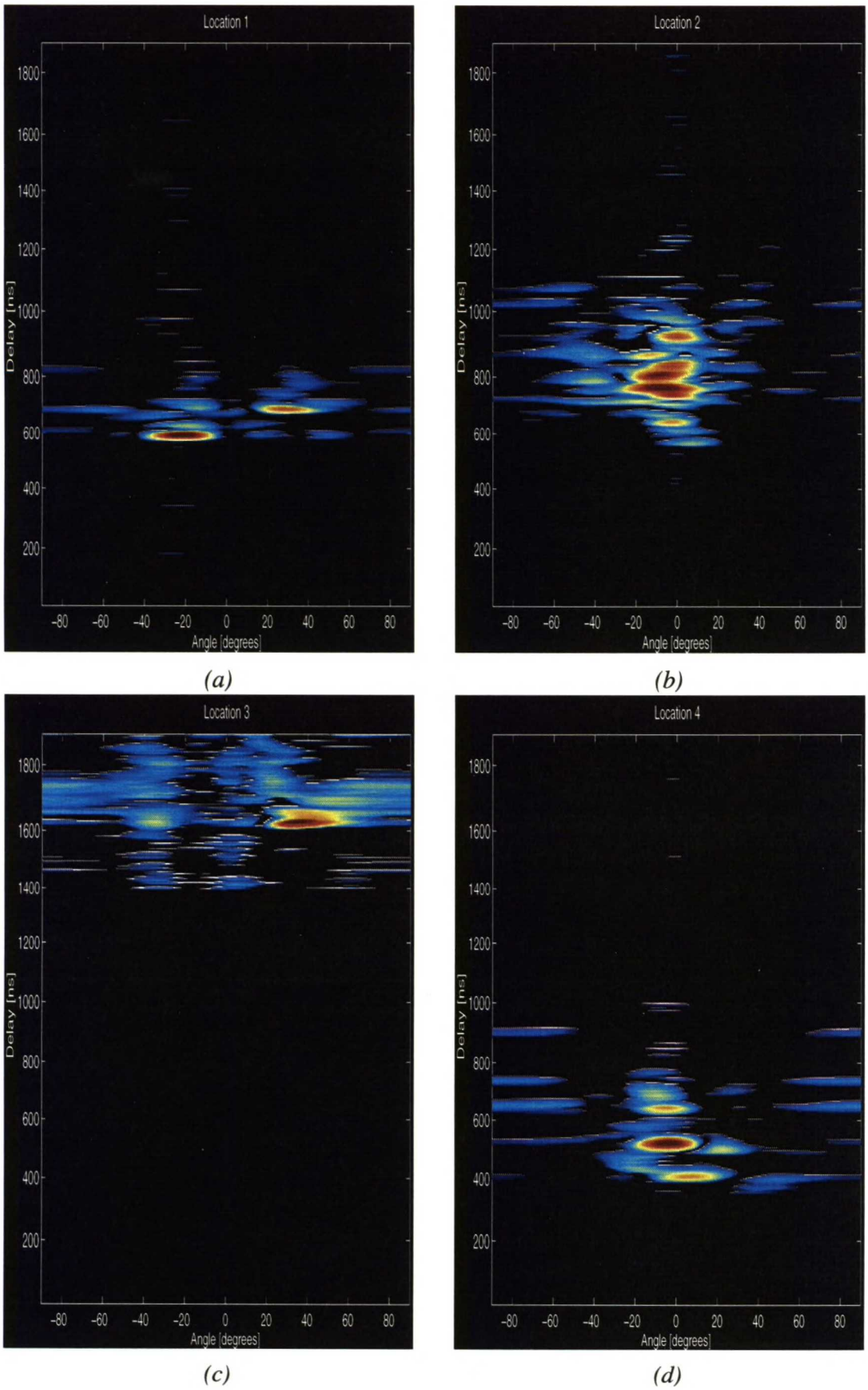

Figure 5.9. *Measured angle and delay distributions of received signals.*

6 Conclusions

Adaptive array antennas like those used at base stations of cellular networks were studied in this master's thesis. The effects of the size and geometry of the array on adaptive antennas were considered. A testbed was built to investigate these effects, and the performance of the testbed was evaluated.

At first the benefits of adaptivity as well as possible approaches to the implementation were discussed. An introduction to array antennas and radiation properties of different array geometries were presented next. Also techniques of pattern optimization v. number of array elements and size of the array were investigated. For example, thinned arrays and array superresolution might provide significant capacity increase compared to the existing systems with moderate cost.

The built testbed is based on a complex wideband radio channel sounder and a fast RF switch. It provides both the incidence angle and delay information of the received signal component and thus allows two-dimensional characterization of the radio channel in realistic environments. The built device can be used in the analysis of antenna arrays and radio channels in various radio systems.

The performance of the testbed was studied by test measurements. The inaccuracy of the measured signal amplitudes was as large as ±1 dB. This is caused by mismatches between the different components of the system including the RF switching unit, feed cables, and antenna elements. One error source is also the overcoupling between the channels of the switch. The internal phase errors of the system consist mainly of the phase noise of the

oscillators and inaccuracy of the calibration of the feed network. The phase errors are less than 3° rms. The phase and amplitude errors limit the capability of the testbed to measure weak effects, such as mutual coupling, in an array under test. Also the synthesis of optimized radiation patterns with low sidelobes requires accurate signal recording. Because of the errors in the feed network, the lowest sidelobe levels achieved with amplitude tapering were of the order of -22 dB.

In addition to the internal errors, the dynamic radio channel causes uncertainty, because the element signals are not measured exactly at the same time. For a maximum beam mispointing of 10 % of the half-power beamwidth, the testbed allows measuring of complex impulse responses for a 16-element array with a delay range of 4.3 μs and 26 m/s mobile speed. The delay resolution can be as good as 17 ns.

The system was tested by practical channel measurements with an 8-element prototype array. The results indicate that the system works well and the components of the received signal with different directions of arrival and time delays can be separated with 13° angular resolution. The developed system provides a novel approach to the two-dimensional analysis of the radio channel.

The main problem with the current setup is that the sliding correlator receiver allows only static measurements. Dynamic measurements will be performed in the future with the direct sampling receiver. Also the accuracy of the testbed will be improved in the future. The errors in the feed network will be reduced by building a better RF switching unit. The system will also be extended for larger numbers of elements. A new array with independent reception of two polarizations is under development. Interesting topics for further studies include e.g. the aperture synthesis technique and adaptive antennas in mobile equipment.

References

[1] R.C. Hansen (ed.), *Microwave Scanning Antennas, Volumes I-III*, New York, Academic Press, 1966.

[2] W.C.Y. Lee, *Mobile Cellular Telecommunications: Analog and Digital Systems*, New York, McGraw-Hill, 1995, 664 p.

[3] J.G. Proakis, *Digital Communications (Third Edition)*, New York, McGraw-Hill, 1995, 928 p.

[4] M.A. Beach, R.L. Davies, P. Guémas, H. Xue, and J.P. McGeehan, "Capacity and Service Extension for Future Wireless Networks Using Adaptive Antennas", *International Conference on Antennas and Propagation*, April 4-7, 1995, pp. 125-129.

[5] P. Zetterberg, "A Comparison of Two Systems for Down Link Communication with Antenna Arrays at the Base", *Submitted to IEEE Transactions on Vehicular Technology.*

[6] G.V. Tsoulos, M.A. Beach, and S.C. Swales, "Application of Adaptive Antenna Technology to Third Generation Mixed Cell Radio Architectures", *Proc. IEEE 44th Vehicular Technology Conference*, Stockholm, Sweden, June 8-10, 1994, pp. 615-619.

[7] J. Fuhl, and A.F. Molisch, "Capacity Enhancement and BER in a Combined SDMA/TDMA System", *Proc. IEEE 46th Vehicular Technology Conference*, Atlanta, GA USA, April 28-May 1, 1996, pp. 1481-1485.

[8] Y. Li, M. Feuerstain, P. Perini, and D. Reudink, "Gain Improvement of a Cellular Base Station Multibeam Antenna", *Proc. IEEE 46th Vehicular Technology Conference*, Atlanta, GA USA, April 28-May 1, 1996, pp. 1680-1684.

[9] T. Rantalainen, *Location of Mobile Station in the GSM network*, Master's thesis, Helsinki University of Technology, September 1995.

[10] J.E. Hudson, *Adaptive Array Principles*, London, IEE, 1981, 253 p.

[11] R.T. Compton, Jr., *Adaptive Antennas, Concepts and Performance*, New Jersey, Prentice Hall, 1988, 448 p.

[12] G.V. Tsoulos, M.A. Beach, and S.C. Swales, "Performance Enhancement of DS-CDMA Microcellular Networks with Adaptive Antennas", *Proc. IEEE 46th Vehicular Technology Conference*, Atlanta, GA USA, April 28-May 1, 1996, pp. 1086-1090.

[13] P.T. Karttunen, T.I. Laakso, and S.J. Ovaska, "Comparison of Howells-Applebaum and the Conventional Beamformer", *Internal Reports*, Helsinki University of Technology, Laboratory of Telecommunications Technology, 1996.

[14] S. Haykin, J. Litva, and T.J. Shepard, *Radar Array Processing*, New York, Springler-Verlag, 1993, 317 p.

[15] S. Haykin, *Adaptive Filter Theory (Second Edition)*, New Jersey, Prentice-Hall, 1991, 854 p.

[16] G.V. Tsoulos, M.A. Beach, and S.C. Swales, "Adaptive Antennas for Third Generation DS-CDMA Cellular Systems", *Proc. IEEE 45th Vehicular Technology Conference*, Chicago, IL USA, July 25-28, 1995, pp. 45-49.

[17] W.C. Jakes, Jr., Y.S. Yeh, M.J. Gans, and D.O. Reudink, "Fundamentals of Diversity Systems", Chapter 5 in *Microwave Mobile Communications*, editor W.C. Jakes, Jr., New York, John Wiley & Sons, 1974, 642 p.

[18] K. Fujimoto, and J.R. James, *Mobile Antenna Systems Handbook*, Boston, Artech House, 1994, 617 p.

[19] J.D. Parsons, and J.G. Gardiner, *Mobile Communication Systems*, London, Blackie, 1989, 292p.

[20] R. Arnott, A. Bull, M. Barrett, A. Carr, "Development of an Adaptive Antenna Demonstrator for DECT", *IEE Colloquium on Smart Antennas,* Savoy Place, London, December 1994.

[21] J. Laiho-Steffens, *Two-dimensional characterisation of the mobile propagation environment*, Licentiate thesis, Helsinki University of Technology, June 1996.

[22] Y. Wang, E. Potter, and J. Saillard, "An Array Antennas of Angular Beam Steering And Polarization Agility", *Proc. IEEE 42nd Vehicular Technology Conference*, Denver CO, USA, May 10-13, 1992, pp. 21-24.

[23] A. Turkmani, A. Arowojolu, P. Jefford, and C.J. Kellett, "An Experimental Evaluation of the Performance of Two-Branch Space and Polarization Diversity Schemes at 1800 MHz", *IEEE Transactions on Vehicular Technology*, Vol. VT-44, No. 2, May 1995, pp. 318-326.

[24] C.R. Ward, J.E. Hudson, and J.G. Searle, "Smart Antenna Solutions for Mobile Radio Systems", *International Conference on Antennas and Propagation*, April 4-7, 1995, pp. 130-136.

[25] O. Nørklit, P.C.F. Eggers, and J.B. Andersen, "Jitter Diversity in Multipath Environments", *Proc. IEEE 45th Vehicular Technology Conference*, Chicago, IL USA, July 25-28, 1995, pp. 853-857.

[26] C. Passerini, M. Frullone, M. Missiroli, and G. Riva, "Performance of Adaptive Antenna Arrays for Wideband Wireless Indoor Communications", *Proc. IEEE 46th Vehicular Technology Conference*, Atlanta, GA USA, April 28-May 1, 1996, pp. 1501-1504.

[27] H. Bach, and J.E. Hansen, "Uniformly Spaced Arrays", Chapter 5 in *Antenna Theory*, editors R.E. Collin, and F.J. Zucker, New York, McGraw-Hill, 1969, 666 p.

[28] I. Lindell, and K. Nikoskinen, *Antenniteoria (Antenna Theory, in Finnish)*, Helsinki, Otakustantamo, 1995, 347 p.

[29] R.J. Mailloux, *Phased Array Antenna Handbook*, Norwood, Artech House, 1993, 524 p.

[30] C. Farsakh, and J.A. Nossek, "On the Spatial Separation Potential of a Uniform Linear Array", *Proc. IEEE 46th Vehicular Technology Conference*, Atlanta, GA USA, April 28 - May 1, 1996, pp. 1477-1480.

[31] A.C. Schell, and A. Ishimaru, "Antenna Pattern Synthesis", Chapter 7 in *Antenna Theory*, editors R.E. Collin, and F.J. Zucker, New York, McGraw-Hill, 1969, 666 p.

[32] J. Litva, and T. Lo, *Digital Beamforming in Wireless Communications*, Boston, Artech House, 1993, 301 p.

[33] C.A. Balanis, *Antenna Theory, Analysis and Design*, New York, Harper & Row, 1982, 790 p.

[34] R. Vescovo, "Pattern Synthesis with Null Constraints for Circular Arrays of Equally Spaced Isotropic Elements", *IEE Proceedings on Microwave Antennas and Propagation*, Vol. 143, No. 2, April 1996, pp. 103-106.

[35] N. Goto, and Y. Tsunoda, "Sidelobe Reduction of Circular Arrays with a Constant Excitation Amplitude", *IEEE Transactions on Antennas and Propagation*, Vol. AP-25, No. 6, November 1977, pp. 896-898.

[36] W.H. Kummer, "Basic Array Theory", *Proceedings of the IEEE*, Vol. 80, No. 1, January 1992, pp. 127-139.

[37] C.S. Ruf, C.T. Swift, A.B. Tanner, and D.M. Le Vine, "Interferometric Synthetic Aperture Microwave Radiometry for the Remote Sensing of the Earth", *IEEE Transactions on Geoscience and Remote Sensing*, Vol. 26, No. 5, September 1988, pp. 597-611.

[38] A.T. Moffet, "Minimum Redundancy Linear Arrays", *IEEE Transactions on Antennas and Propagation*, Vol. AP-16, No. 2, March 1968, pp. 172-175.

[39] Y. Wang, and J.R. Cruz, "Augmented Antenna Arrays for CDMA Cellular Systems", *Proc. IEEE 46th Vehicular Technology Conference*, Atlanta, GA USA, April 28-May 1, 1996, pp. 1091-1095.

[40] T. Rouphael, and J.R. Cruz, "Enhanced CDMA Cellular System Using Interpolated Circular Arrays", *Proc. IEEE 46th Vehicular Technology Conference*, Atlanta, GA USA, April 28-May 1, 1996, pp. 1071-1075.

[41] D.M. Pozar, "A Review of Bandwidth Enhancement Techniques for Microstrip Antennas" in *Microstrip Antennas, The Analysis and Design of Microstrip Antennas and Arrays*, editors D.M. Pozar, and D.H. Schaubert, New York, IEEE Press, 1995.

[42] J.-F. Zürcher, and F.E. Gardiol, *Broadband Patch Antennas*, Boston-London, Artech House, 1995, 209 p.

[43] D.R. Jackson, J.T. Williams, A.K. Bhattacharyya, R.L. Smith, S.J. Bucheit, and S.A. Long, "Microstrip Patch Designs That Do Not Excite Surface Waves", *IEEE Transactions on Antennas and Propagation*, Vol. AP-41, No. 8, August 1993, pp. 1026-1037.

[44] D.L. Margerum, "Self-Phased Arrays", Chapter 5 in *Microwave Scanning Antennas, Vol III: Array Systems*, editor R.C. Hansen, New York, Academic Press, 1966, 422 p.

[45] B. Ottersten, "Spatial Division Multiple Access (SDMA) in Wireless Communications", *Proc. Nordic Radio Symposium*, Salsjöbaden, Sweden, April 24-27, 1995.

[46] J.L. Butler, "Digital Matrix, and Intermediate-Frequency Scanning", Chapter 3 in *Microwave Scanning Antennas, Vol III: Array Systems*, editor R.C. Hansen, New York, Academic Press, 1966, 422 p.

[47] R.C. Hansen, "Fundamental Limitations in Antennas", *Proceedings of the IEEE*, Vol. 69, No. 2, February 1981, pp. 170-182.

[48] E.H. Newman, J.H. Richmond, and C.H. Walter, "Superdirective Receiving Arrays", *IEEE Transactions on Antennas and Propagation*, Vol. AP-26, No. 5, September 1978, pp. 629-635.

[49] W.F. Gabriel, "Adaptive Processing Array Systems", *Proceedings of the IEEE*, Vol. 80, No. 1, January 1992, pp. 152-162.

[50] H. Steyskal, and J. Herd, "Mutual Coupling Compensation in Small Array Antennas", *IEEE Transactions on Antennas and Propagation*, Vol. AP-38, No. 12, December 1990, pp. 1971-1975.

[51] I.J. Gupta, and A.A. Ksienski, "Effect of Mutual Coupling on the Performance of Adaptive Arrays", *IEEE Transactions on Antennas and Propagation*, Vol. AP-31, No. 5, September 1983, pp. 785-791.

[52] Y.T. Lo, and S.W. Lee, *Antenna Handbook, Vol. III, Antenna Applications*, New York, Van Nostrand Reinhold, 1993.

[53] J. Kivinen, *Nopea laajakaistaisen impulssivasteen mittaus (Rapid broad band radio channel impulse response measurement, in Finnish)*, Master's thesis, Helsinki University of Technology, June 1995.

[54] R. Gruber, *Planning and Programming Data Acquisition Equipment for a Wideband Mobile Channel Measurement System*, Diploma thesis, Helsinki University of Technology, December 1994.

[55] P. Aikio, *Radiokanavaluotaimen kehittäminen (Development of the radio channel sounder, in Finnish)*, Master's thesis, Helsinki University of Technology, February 1996.

[56] J. Talvitie, *Wideband Channel Measurement for VHF and UHF Mobile Communications*, Licentiate thesis, University of Oulu, June 1993.

[57] F. Dolley, "Fast Sounding of Broadband Radio Channel at 2 GHz Frequency Range", Project Report, Helsinki University of Technology, Radio Laboratory, June 1996.

[58] Data obtained from J. Kivinen, Helsinki University of Technology, Radio Laboratory, February 1997.

[59] L.E. Larson (ed.), *RF and Microwave Circuit Design for Wireless Communications*, Boston, Artech House, 1996, 411 p.

Appendix A: Transmitter locations in practical measurements

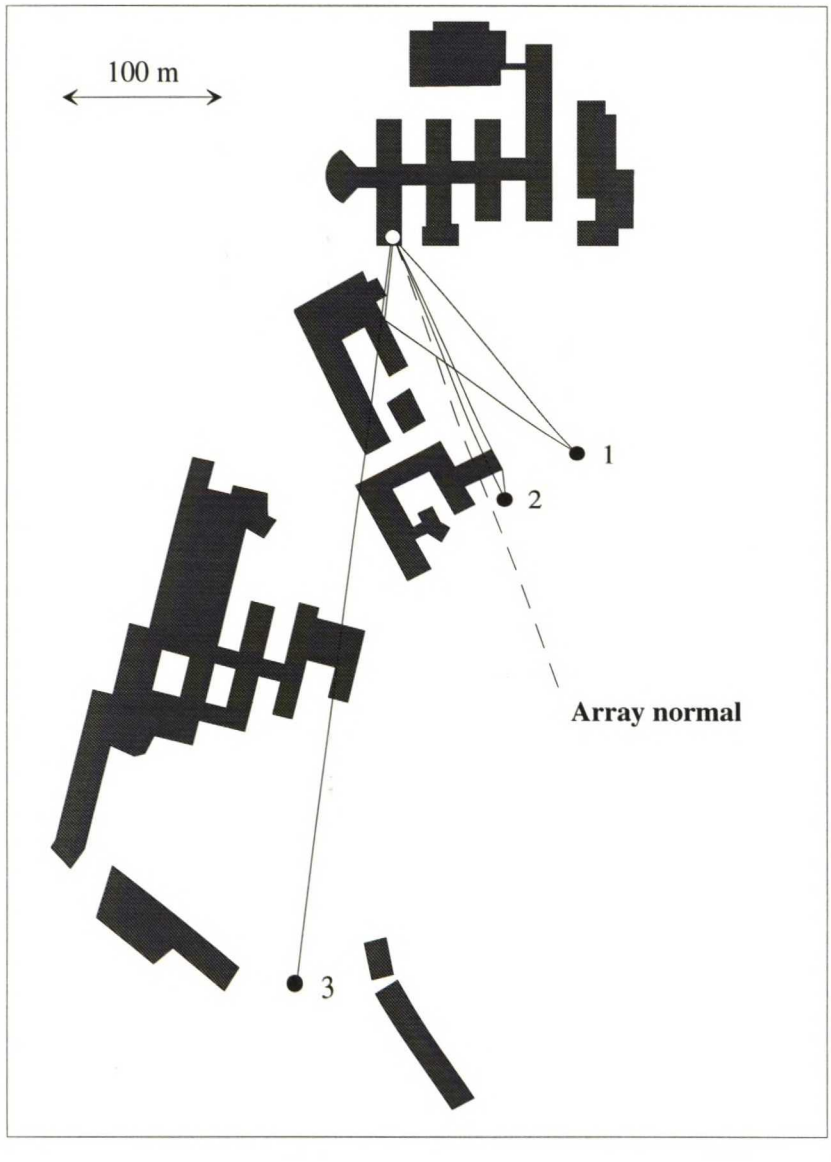

Figure A-1. *Transmitter locations 1-3.*

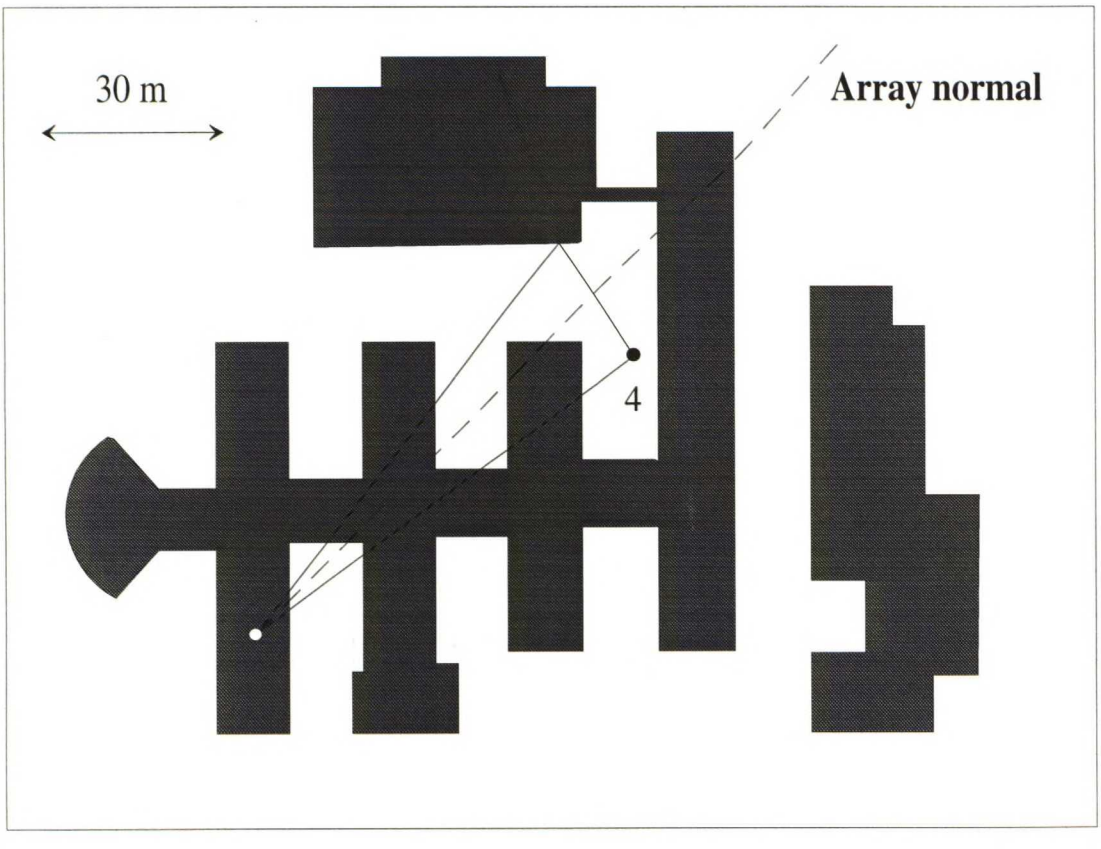

Figure A-2. *Transmitter location 4.*